Electrochemical Investigation of Platinum Nanoparticles Supported on Carbon Nanotubes as Cathode Electrocatalysts for Direct Methanol Fuel Cell

Asanda Ntlauzana

A thesis submitted in fulfillment of the requirements for the degree of Magister Scientiae in the Department of Chemistry, University of the Western Cape.

Supervisor: Dr. L. Khotseng

Co-Supervisor: Dr P. Ndungu

November 2010

DECLARATION

I declare that "Electrochemical Investigation of Platinum Nanoparticles Supported on Carbon Nanotubes as Cathode Electrocatalysts for Direct Methanol Fuel Cell" is my own work, that it has not been submitted for any degree or examination in any other university, and that all the sources I have used or quoted have been indicated and acknowledged by complete references.

Asanda Ntlauzana November 2010

Signed:…….

ABSTRACT

The investigation of supported platinum electrocatalyst was conducted on the search for global interest in direct methanol fuel cell (DMFC), national strategies in beneficiation of platinum (Pt) and understanding the electrochemical properties of supported Pt nanoparticles as electrocatalysts. Two sets of Multi-walled carbon nanotubes, liquid petroleum gas and ethylene synthesized Multi-walled carbon nanotubes (LPGMWCNT and EMWCNT) with an outside diameter range of 16 - 75 and 21- 85 nm respectively, were synthesized by chemical vapor deposition (CVD). Platinum was deposited on the nanotubes using hexachloroplatinic acid (H_2Cl_6Pt) · $6H_2O$ as a precursor and ethylene glycol (EG) as the solvent and reducing agent. Isopropanol was also used to investigate the effect of different solvents on the reduction and deposition of platinum nanopaticles on the CNT support material. Commercial MWCNT were also used to compare the results. X-ray diffraction (XRD) and TEM data (50 particles were counted) was used to calculate the particle size of the Platinum metal deposited on MWCNT. Particle sizes of 2.8, 2.5 and 2.75 nm for Pt/EMWCNT, Pt/LPGCNT and Pt/ commercial CNT respectively, were obtained from the TEM data which was in agreement with XRD.

The particles of the Pt metal were well dispersed on carbon nanotubes when EG was used and in isopropanol poor dispersion was observed and no further investigation was done on them. The platinum wt% on the supports observed from EDS was 21.8, 19.10 and 16.74wt% for Pt/EMWCNT, Pt/LPGCNT and Pt/ commercial CNT respectively.

Pt/LPGMWCNT showed high electro-catalytic activity of 2.48 mA and active surface area of 76 m^2/g, toward oxygen reduction, observed from cyclic voltammogram in

sulfuric acid. Pt/LPGMWCNT also showed better tolerance toward methanol, however it was not highly active towards methanol, and hence the methanol oxidation peak current observed between 0.75 and 08 potential was the smallest.

In this study a wide range of instruments was used to characterize the properties and behavior of Platinum nanoparticles on multi-wall carbon nanotubes. To add to the already mentioned, Scanning electrochemical microscopy (SEM), proton induced x-ray emission (PIXE), scanning electrochemical microscopy (SECM) and Brunauer-Emmett Tellar (BET) were also used

ACKNOWLEDGEMENTS

I would like to thank and give prays to my God Almighty for the favor and grace He has granted me, for if it was not him I would not be where I am. For His continuing patience and grace over my life.

Greatest gratitude to both my parents, Buyiswa Ntlauzana, Zolisa Mayekiso and to my sister Yanela Ntlauzana, for the support, love and encouragement they give me into being the best that I can be.

Prof. V.M. Linkov, Dr. L. Khotseng, and the staff of the South African Institute for Advanced Materials Chemistry for giving me an opportunity to conduct the research in the Institute.

A special thanks to Dr. P. Ndungu for all the help guidance and for his insight into thesis writing.

Mr. A. Josephs (Electron Microscopy Unit, Department of Physics, University of the Western Cape) for helping with Scanning Electron Microscopy, Transmission Electron Microscopy.

Dr. R. Bucher, Dr. M. Nkosi and Dr.W. Przybylowicz (Materials Research Group, iThemba Labs) for measurements and assistance with X-Ray Diffraction, Atomic Force Microscopy and Proton-Induced X-ray Emission Spectroscopy respectively.

My sincere thanks to Wafeeq Davids for helping with the Production of Carbon nanotubes, Marvin Piet for helping me with CV and his support through out my research and during hardships with my studies, Stanford Chidziva for assistance with the use of instruments, and Nolubabalo Matinise for helping with the experimental work.

A huge thanks and appreciation to my colleagues and friends, Ncumisa Jonas, Bulelwa Ntsendwana, Oko Gcilitshana and to all my friends for their support during the course of study.

The financial assistance of the National Research foundation (NRF) and ESKOM (TESP) towards this research is hereby acknowledged.

TABLE OF CONTENTS

LIST OF FIGURES

LIST OF TABLES

ABBREVIATIONS

BET	Brunauer-Emmett-Teller
CNT	Carbon Nanotube
CV	Cyclic Voltammetry
CVD	Chemical Vapor Deposition
DMFC	Direct Methanol Fuel Cell
EDS	Energy Dispersive Spectroscopy
LPG	Liquefied Petroleum Gas
MWCNT	Multi-wall Carbon Nanotube
ORR	Oxygen Reduction Reaction
PEMFC	Polymer Electrolyte Membrane Fuel Cell
PIXE	Proton Induced X-ray Emission
SEM	Scanning electron Microscopy
SECM	Scanning Electrochemical microscopy
TEM	Transmission Electron Microscopy

UME	Ultra-Micro Electrode
XRD	X-Ray Diffraction

INTRODUCTION: MOTIVATION AND OBJECTIVES OF THE STUDY

1.1 BACKGROUND TO ENERGY SOURCES

Globally, the demand for energy is ever increasing. The use of coal, oil or any hydrocarbon fuel leads to the generation and release of carbon, nitrogen and sulfur oxide gases into the atmosphere causing air pollution and ozone layer depletion. It has been observed that the ozone in the earth's atmosphere is deteriorating and has a big hole on it, which will allow the transmission of more harmful ultraviolet rays to the environment [1]. Chlorofluorocarbons (CFC) and nitrogenous oxides are responsible for the deterioration of ozone [2]. On the other hand, emission of CO_2 gas into the atmosphere has been linked to global warming [3]. So, to avoid generation of carbon monoxides, carbon dioxide and other harmful pollutants, there is a direct need to look at alternate sources of energy that favors cleaner fuels. Examples include fuel cells, solar technologies (photovoltaics, concentrating mirrors, etc), wind turbines, tidal systems etc, have been under investigation for this use but fuel cells are one of the emerging technology that can meet these demands. Other alternative technologies include bio-fuels, hybrids (solar electric, battery petrol, etc). Fuel cells would dramatically reduce air pollution as they produce only water as the byproduct after combustion, and when using hydrogen or carbon source from renewable sources can decrease oil dependency. Fuel cells can provide safer, cleaner and more energy efficient power systems and provide new business opportunities. If we pollute the atmosphere, the entire planet is at stake. To buy the necessary time fuel cell technology can act as an intermediate technology as it will reduce pollution levels considerably. Another advantage of fuel cells is the sustainable energy conversion they offer in both stationary and mobile power applications. Since

fuel cells operate silently they reduce noise pollution, while the waste heat from a fuel cell can be used to provide hot water or space heating.

One of the factors driving the research and development of the fuel cells is the use of energy sources with environmentally friendly product. Hydrogen (H_2) is one of the most important of all available energy carriers that can be used. Its ability to produce more energy than any other fuel; its universal availability, simple and clean conversion to heat makes it a better supply of energy. Most of the hydrogen is locked up in various chemicals, water and hydrocarbons. One way to obtain hydrogen is to extract it from water through a process called electrolysis. In this process energy is applied to dissociate water molecules to hydrogen and oxygen.

1.2 RATIONAL TO THE RESEARCH

The direct methanol fuel cell (DMFC) which is a low temperature fuel cell has attracted considerable attention for portable power applications and posses a number of advantages. The use of liquid fuel is considered to be essential for commercial use because it can be easily transported and stored, less safety concern, and relatively small investment needed for placing the relevant support infrastructure. Another advantage is that these fuel cells can achieve efficiencies of up to 40%. DMFCs are available at very high cost because of the electrocatalyst used which is platinum based and can be very expensive. This can be overcome by using reduced amounts of the catalyst without reducing the efficiency of the cell or using non – platinum based catalysts. Methanol crossover from the anode side to the cathode is also one of the main hurdles for the development of DMFC to reach its full commercialization potential due to the fact that commonly used Platinum (Pt) cathode catalyst are also very active to methanol oxidation and

methanol oxidation tend to also occur on the cathode electrode. Consequently this does not only lowers fuel utilization efficiency but also decreases the cathode performance. Another problem is the irreversibility of the oxygen reduction reaction. Many works have sought for more active electrode catalysts and have addressed ways to increase the dispersion of such catalysts to promote methanol oxidation. They have also considered the modification of Nafion membranes and development of new proton conducting polymers for reduction of methanol crossover. To avoid methanol crossover problems, except for the efforts for developing novel and less permeable membranes, another effective route may be utilization of oxygen reduction catalyst with enhanced oxygen reduction activity and high methanol tolerance. Thus, great efforts are being made towards development of alternative electrocatalyst with high oxygen reaction activity, high methanol tolerance and low catalyst content. These catalysts can be obtained by using high surface area nanocomposite materials as supports for the catalyst metal. Typically the supports for these catalysts are usually carbon based and a relatively new type of support that poses high quality and enhanced properties are carbon nanotubes.

Testing and characterization of metal catalyst include evaluating the active metal surface area, dispersion, and metal nanocluster size and catalyst activity. Particle size of these electrocatalysts is usually decreased to the nanometer range to increase the surface area of the metal catalyst as well as exploiting materials tendency to gain improved or new properties. Different properties of electrocatalysts such as particle size and dispersion on the supporting material have been characterized and are believed to increase the efficiency of the fuel cells. New nanoparticle electrocatalyst should have enhanced physical-chemical properties compared to the existing commercial catalysts to be considered for future applications in fuel cells. Focus has to be toward

the identification of properties that influence the behavior of nanometer range electrocatalysts. A minimum set of characterization techniques such as X-ray diffraction (XRD), X-ray photoelectron spectroscopy (XPS), scanning electron microscopy (SEM), Transmission electron microscopy (TEM), etc. are considered as the commonly used and essential.

DMFCs are available on a limited scale; methanol fuel has an energy density that is lower than current petrol used and slightly lower than hydrogen. But, because methanol is a liquid, it can be easily integrated into existing fuelling infrastructure. DMFC systems are much more efficient than combustion engines, quieter and less polluting. But despite these advantages DMFC suffer from methanol cross-over problems and there is a room much more improvement in terms of catalysts development.

1.3 OBJCTIVES OF THE STUDY

The main objective of this study is to synthesize and investigate thephysical - chemical properties of carbon nanotubes, platinum dispersed on carbon nanotubes (Pt/CNT) and the applicability of Pt/CNT in DMFC systems. The aim is to study the electrode surface structure \and electrochemical properties of the Pt/CNT using cyclic voltammetry. The main sub-objectives of the study include:

- Synthesis of carbon nanotubes
- Characterization of CNT using scanning electron microscopy, transmission electron microscopy, X-ray diffraction, nitrogen sorption at 77K and atomic force microscopy.
- Synthesis of platinum nanoparticles dispersed on carbon nanotubes (Pt/CNT)

- Physical and chemical characterization of platinum supported catalyst (Pt/CNT)
- Evaluate the effect of different preparation conditions of Pt/CNT on the physical – chemical properties

1.4 FRAME WORK OF THE STUDY

Carbon nanotubes will be synthesized using chemical vapor deposition (CVD) synthesis method, purified and used as support material for Pt nanoparticles. In addition commercial platinum on carbon (Pt/C) will be characterized and used for comparison. The various Pt/CNT will be fully characterized using a number of techniques.

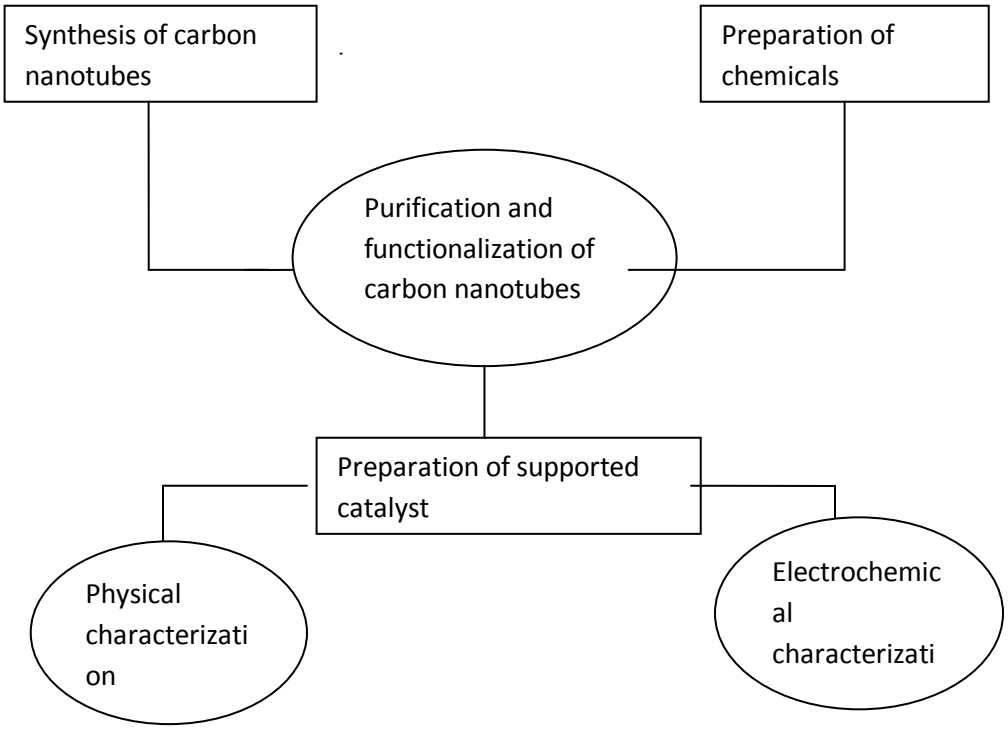

Figure 1.1 *Process scheme for research frame work.*

1.5 RESEARCH OUTLINE

Chapter two: Literature review

This chapter starts with an introduction to fuel cells, types and operation conditions are also stated. The main focus of the chapter is on DMFCs, and includes advantages, operating principles and challenges. The chapter also goes into detail about the electrocatalysts used by DMFCs, the attempts that have been made by other scientists to increase the activity and durability of these catalysts and on the reactions that take place on the anode and cathode electrodes of the fuel cell with particular attention on the ORR. Properties of the catalyst and the support material are also discussed on this chapter.

Chapter Three: Experimental work

Chapter 3 describes the chemicals, preparation methods and instruments that were used during this investigation. Brief basic information about the characterization techniques used in the study is given after the introduction to the chapter. Insight about the type of information that can be acquired is also included.

Chapter four: Results and Discussion

Chapter 4 provides the results for the structural, physical and electrochemical characterization of the synthesized platinum nanoparticles dispersed on carbon nanotubes (Pt/CNT) and commercial Pt/C.

Chapter five: Conclusion and Recommendations

The final conclusion on the optimum method for preparation of the most active catalyst drawn from the results obtained during characterization after comparing all the material and the properties is stated in this chapter. Recommendations are also described in this chapter.

2. LITERATURE REVIEW

This chapter discusses the role of characterization study of electrocatalysts, synthesis of support materials and their application. The main focus is on the discussion of physical-chemical and electrocatalytic properties of electrocatalysts in a nanometer domain for application on direct methanol fuel cell cathode electrode (DMFC). The literature is also focused on (DMFC) electrode catalysts and the use of supported electrocatalysts in the cathode electrode to improve activity, their role and reactions facilitated by these electrocatalysts at the electrodes. The effect of the methanol that passes through the polymer membrane is also addressed in the literature. A detailed and minimum set of physical-chemical properties influencing the behavior of these materials is identified. Physical-chemical areas of the electrocatalyst that require extensive investigation are also revealed. Support and supported electrocatalysts are synthesized and characterized to investigate their physical-chemical properties. Platinum was chosen as the metal catalyst for the DMFC cathode electrode as the literature reveal that it is the most active of the transition elements for cathode reactions.

2.1 OVERVIEW TO FUEL CELLS

The first fuel cell was discoverd by Sir William Grove in 1839, and he is widely acknowledged as the “Father of Fuel cells”. Grove was interested in reversing the process of electrolysis which is precisely what happens in fuel cells [4, 5]. Fuel cell is defined as an electrochemical energy conversion device that produces electricity by converting the chemical energy of fuel and oxidant, which react in the presence of a catalyst, to electrical energy. It is possible to continuously provide the fuel and oxidant into the fuel cell and is a characteristic that makes it

different from other devices such as Batteries. Conversion of chemical energy in fuel cells is directly to electrical energy while in combustion engines chemical energy is first converted to mechanical energy then to electrical energy. A schematic diagram is given in Figure.2.1 showing different energy conversion paths corresponding to fuel cells and combustion engines and equation 2-1 is a general equation for energy production from the reaction of hydrogen and oxygen producing water and energy as heat which is called reverse electrolysis.

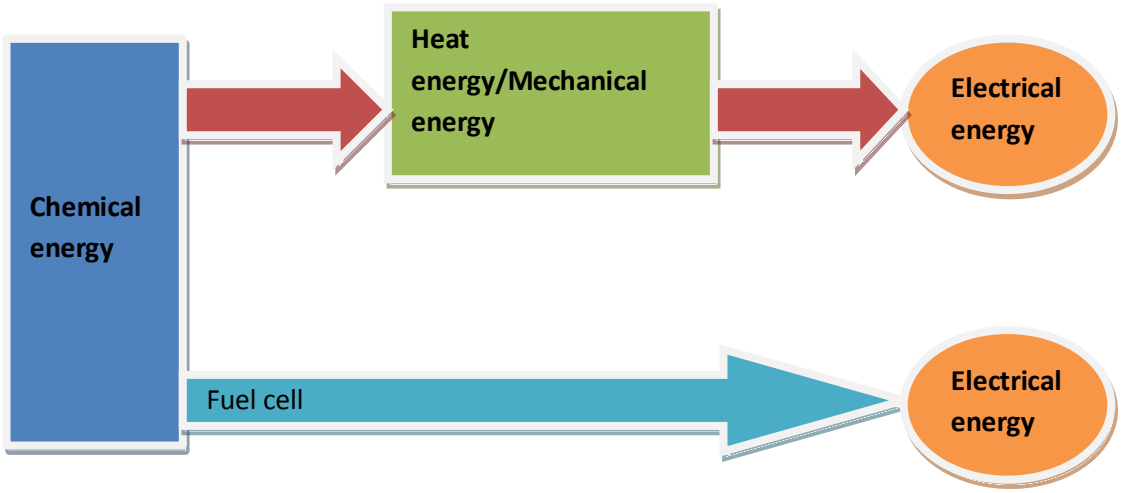

Figure.2. 1 *Different energy conversion paths.*

$$2H_2 + O_2 \rightarrow 2H_2O \qquad \Delta H = -572kj$$ Equation: 2-1 [6]

These devices are considered as energy converters, analogous to combustion engines and are an alternative to other power sources (coal, oil and natural gas) as they show higher energy conversion efficiency due to the direct conversion of chemical energy into electrical energy and environment-friendly working characteristics [7]. The primary components of a fuel cell are an anode electrode, a cathode electrode and an ion conducting electrolyte, collectively known as

membrane electrode assemble (MEA) as shown schematically on Figure2.2. Oxidation of the fuel takes place on the anode and reduction occurs on the cathode of the fuel cell. The membrane is often referred to as the heart of the fuel cell, and its main purpose is to act as a proton conductor and also as a fuel barrier separating methanol or hydrogen and oxygen. Important membrane properties are low gas permeability, high proton conductivity and sufficient mechanical and chemical stability [8, 9].

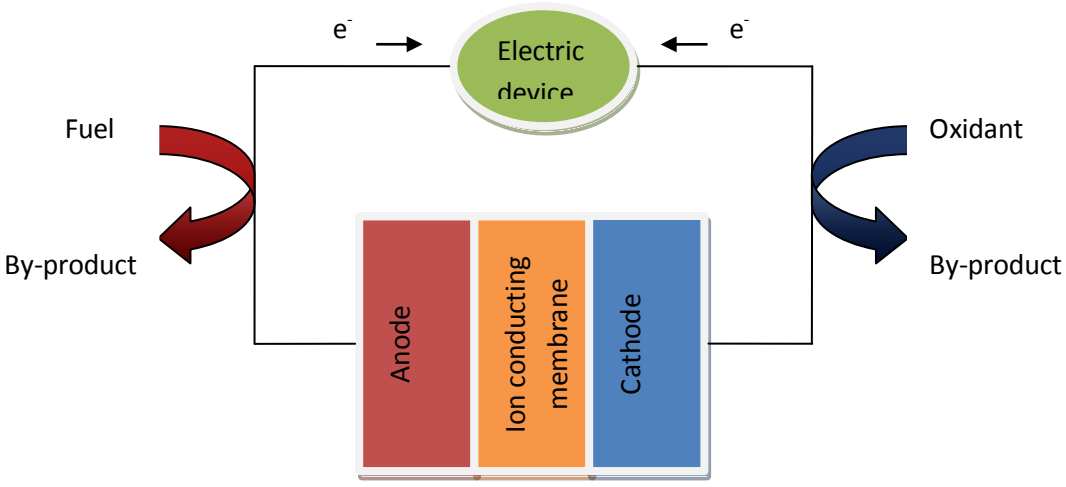

Figure 2.2 *General Schematic diagram of a fuel cell.*

There are five classes of fuel cells which have received the greatest amount of attention in terms of research throughout the world; these devices are identified by the type of electrolyte used and operating temperature. There are also other types of fuel cells such as zinc air fuel cell (ZAFC), protonic ceramic fuel cell (PCFC) and microbial fuel cell (MFC) [10]. Although the naming is based on the type of electrolyte used, there are other important differences as well. Each fuel cell class differs in material, construction and fabrication technique for each system. The potential

application of these cells depends on the characteristics of each class of fuel cells [11, 12]. Below are the names and brief description on the five types of fuel cells.

Solid Oxide Fuel Cell (SOFC, 750-1000°C). The operation of the first ceramic SOFC at 1000°C was in 1937 by Baur and Preise who started experimenting with this type of fuel cell in the late 1930s[13]. A SOFC consists of two electrodes sandwiched around a ceramic electrolyte such as Zirconia. Several ceramic materials are employed as electrolyte for active SOFC, although a variety of oxide combination has been used for solid non-porous electrolytes, the most common has been Zicornia. Hydrogen is fed on the anode and oxygen, from air, on the cathode. SOFC anodes are fabricated from composite powder mixtures of electrolyte material and nickel oxide (NiO). NiO/YSZ anode material is suited for applications with YSZ (yttrium-stabilized zirconia) electrolyte [14]. Noble metals or electronic conducting oxide are used as cathode materials because of high operating temperatures. Perovskites- type lanthanum strontium manganite ($LaSrMnO_3$) offer excellent thermal expansion mach with zirconia electrolytes and provide good performance at operating temperatures above 800°C [15]. SOFC are currently operating, Siemens Westinghouse has tested several tubular prototype systems with excellent results. A plant in Netherlands has been operated for more than two years and earlier prototype installation has been operating for 8 years [16].

Molten Carbonate fuel Cell (MCFC, 650-700)**.** MCFC are high temperature systems which use an immobilized liquid molten carbonate salt suspended on a matrix as the electrolyte. The matrix of the MCFC has to be composed of porous and electronically insulating material which is almost insoluble in the melt [17]. Commonly used salts include lithium, potassium and sodium carbonates. Upon heating the salts form carbonate ions which then flow from cathode toward the

anode where they combine with hydrogen to form water, carbon dioxide and electrons. The electrons are passed through an external circuit producing electricity. At the cathode, oxygen and recycled carbon dioxide from the anode react with the electrons to form carbonate ions that replenish the electrolyte [18]. Anode is a highly porous sintered nickel powder alloyed with chromium to prevent agglomeration and creep at operational temperatures. The cathode is a porous nickel oxide material doped with lithium [19]. One advantage of MCFCs is that they are not prone to carbon monoxide poisoning because of their high operating temperatures. There are a number of MCFC manufactures considered as major developers in the world. These include, fuel cell energy (FCE in USA), Ansaldo Fuel Cell (AFCo in Italy), Ishikawajima-Harima Heavy Industries (IHI, Japan), CFC solutions in Germany etc. Fuel cell systems based on MCFC technology are under development in Italy, Japan, Korea, USA and Germany. Since the 1990s, MCFC systems have been tested in field trials in the range between 40 kW and 1.8 MW [20].

Phosphoric Acid Fuel Cell (PAFC 190-210℃)**.** PAFC were developed from the 1970s through the 1990s by several companies in the United States, including ONSI, a division of international fuel cells (IFC). Phosphoric acid, (H_3PO_4) in high concentration (90-100%) is used as the electrolyte in PAFC because of its good thermal, chemical and electrochemical stability [21]. In PAFC, carbon supported platinum catalysts the most commonly used for both, oxidation of hydrogen fuel at the anode and oxygen reduction at the cathode (The first PAFC plants were first tested in the early 1990's, and a PC25C power plant was installed and commissioned during the turn of the year 1996/1997 by the Erdgas-Energy-System [22]. UCT fuel cells installed a 200kW unit PAFC fuelled by natural gas at New York City's central park heard quarters in Manhattan [23].

Alkaline fuel cell (AFC, 90-200℃). AFC were used in the 1960s and 1970s by NASA in the Apollo and space shuttle programs [24]. This type of fuel cell uses an alkaline solution such as potassium hydroxide (KOH) as electrolyte and a wide selection of possible electrocatalysts like platinum, nickel, iron and aluminum with platinum receiving the most interest for both the anode and cathode. Hydrogen, methanol, ethanol and sodium borohydride have been employed as fuel [25]. ELENCO, in Belgium developed the first AFC with circulating electrolyte until 1996 [26].

Polymer Electrolyte Fuel Cell (PEFC, 65-85℃). Polymer electrolyte fuel cells employ a polymer membrane with acid side groups to conduct protons from anode to cathode. The most common polymer electrolytes used in-PEFCs are perflouro-sulfonic acid (PFSA) ionomers such as Nafion, which are available in films of thicknesses varying from 25 to175 μm. The electrodes are typically made from platinum or platinum alloy supported on carbon with an appropriate amount of ionomer added to bind each electrode and promote protonic activity [27]. Polymer electrolyte membrane fuel cells (PEMFC) are currently used by many companies for small stationary power plants and in automobile application. PEMFC were first developed by General electric company which maintained a high level of interest in fuel cell sector [28].

The operation conditions of the five fuel cells are summarized in **Table 2.1** bellow.

Table 2.1 Five types of fuel cells [29].

	SOFC	**MCFC**	**PAFC**	**AFC**	**PEMFC**
Type of electrolyte	O^- ions (stabilized ceramic matrix with free oxide ions)	CO_3^- ions (typically, molten $LiKaCO_3$ eutectics)	H^+ ions (H_3PO_4 solutions)	OH^- ions (typically aqueous KOH solution)	H^+ ions (with anions bound in polymer membrane)
Type of construction	Ceramic, high temp metals	High temp metals, porous ceramic	Carbon porous ceramics	Plastic, metal	Plastic, metal or carbon
Internal reforming	Yes, good temp match	Yes, good temp match	No	No	No
Oxidant	Air	Air	Air to enriched air	Purified air to O_2	Air to O_2
Operational Temperature	750-1000℃	650-700℃	190-210℃	90-260℃	65-85℃
DC System level efficiency %	45-55%	40-50%	35-45%	32-40%	25-35%

Primary Contaminate Sensitivity	Sulfur	Sulfur	CO < 1%,	CO,CO_2 and Sulfur	CO, Sulfur and NH_3

In addition to the five classes of fuel cells, there are other types of fuel cells not classified by the type of electrolyte. These are the, direct methanol fuel cells (DMFCs) and microbial fuel cells which are distinguished by the type of fuel used and Regenerative Fuel Cell (RFC), distinguished by its operational method.

Out of these fuel cells, two of them are considered as the most interesting fuel cells because of their low operating temperatures and efficiency [9], that is the direct methanol fuel cell (DMFC) and polymer electrolyte membrane fuel cell (PEMFC). The most important aspect about fuel cells it that they generate electricity with little or no pollution to the environment. The oxygen and hydrogen that are used to generate electricity combines to form a harmless byproduct which is water [10]. The DMFC uses methanol which has high energy density than hydrogen and is liquid, making it easy to adapt into existing fuel infrastructure to the advantage of its application in small and portable devices [30]. DMFC uses platinum electrocatalysts, Pt is a strategic resource in RSA, thus a need to carry out extensive research and development on Pt benefication (national priority) These interesting characteristics of the direct methanol fuel cell contributed on it selected to be the main focus of this study with the cathode electrode catalyst being the main area of study.

2.2 DIRECT METHANOL FUEL CELL

The direct methanol fuel cell has several advantages which makes it suitable for applications in ground transportation, portable and electronic devices, including high efficiency, very low emissions, low temperatures, a potentially renewable fuel source and fast convenient refueling [31].The direct methanol fuel cell operates at low temperatures (up to 150°C) and is fed with an aqueous solution of methanol. Cell operation in gas phase also gives good performance. However, need for vaporization may be a limitation for some applications when gas phase fuel is used. The liquid fed system can be operated even at room temperatures and does not need complex humidification and heat management modules as hydrogen fed fuel cell. Humidification and heat regulation is provided by circulating the methanol –water mixture. These advantages allow DMFCs to be customized for use in portable electronic devices [32]. The only disadvantage of methanol use as fuel in fuel cell technology is methanol crossover. Methanol tends to diffuse to the cathode side where there is an oxidant (oxygen) and methanol oxidation occurs on the cathode catalyst, thus reducing the performance of the cell.

The use of methanol has several advantages in comparison to hydrogen:

- It is a cheap liquid fuel
- Easily handled
- It is easy to transport and store
- Has high theoretical energy density of 6100$WhKg^{-1}$ [33]

2.2.1 OPERATING PRINCIPLE OF THE DIRECT METHANOL FUEL CELL

The DMFC is a specialized PEMFC that operates on methanol instead of hydrogen on the anode side. It consists of several layers. The three key layers include; 1) the membrane electrode assemble (MEA) which is formed by the electrodes (anode and cathode), a proton conducting membrane and the catalyst. 2) a catalyst layer and 3) the other part of the fuel cell is hardware as shown in Figure 2.3.

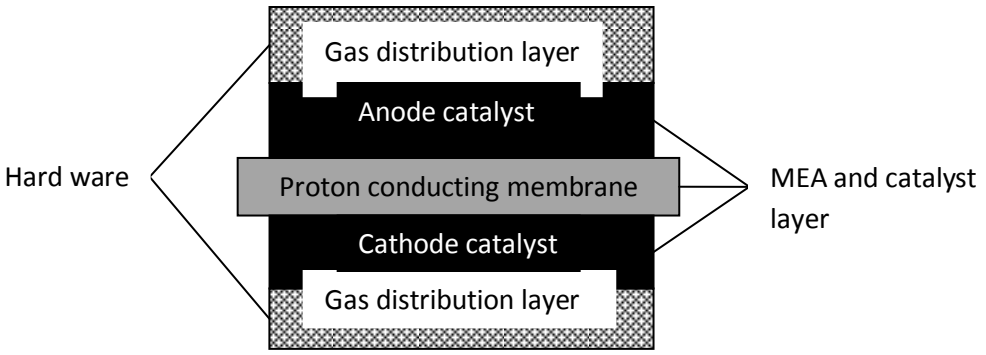

Figure 2.3 *key components of a DMFC.*

Typical anode and cathode catalysts are nanostructured Platinum Ruthenium (Pt-Ru) and Pt particles dispersed on a conductive carbon support respectively. The proton conducting electrolyte normally employed is the polymeric membrane called Nafion©, which is a hydrated perflorosulfonic acid polymer. The hardware consists of the backing layers, flow fields and current collectors designed to maximize current collection from the MEA. The backing layers next to the electrodes are usually made of a porous carbon paper or carbon cloth, about as thick as 4-12 sheets of paper. The backing layer has to be made of material that can conduct electrons leaving the anode to the cathode. Backing layer also helps in water management in the fuel cell. The correct backing material allows the right amount of water vapor to reach the MEA and keep

it humid. They are often coated with Teflon^{TM} to ensure that the pores in the backing material do not become clogged with water, which would prevent rapid gas diffusion necessary for good reaction rate at the electrodes [34, 35]. There is a piece of hardware called a 'bipolar plate' at each outer side of the backing layer that serves as both flow field and current collector which are made of lightweight, strong, gas-impermeable, electron conducting material. The commonly used materials for bipolar plates are graphite, metals and recently developed composite plates. Bipolar plates are responsible for the fuel and water flow in the fuel cell stack. The bipolar plates have different channel flow pattern which is believed to have direct influence on the fuel cell performance. Serpentine flow pattern has the best results based on practical tests compared to other patterns(like parallel flow field pattern) as it contributes to better CO_2 exhaust on anode side, low methanol crossover, high fuel utilization and slightly larger voltage efficiency at low current densities [36, 37].

During cell operation protons and electrons are produced at the anode by oxidation of methanol with the assistance of the electrocatalyst. The protons then migrate to the cathode through the Nafion© membrane while the electrons flow through the external circuit towards the cathode. Electrons and protons react with the oxygen molecules on the cathode electrode to produce water as a byproduct [38]. Figure 2.4 shows the Schematic diagram of the direct methanol fuel cell.

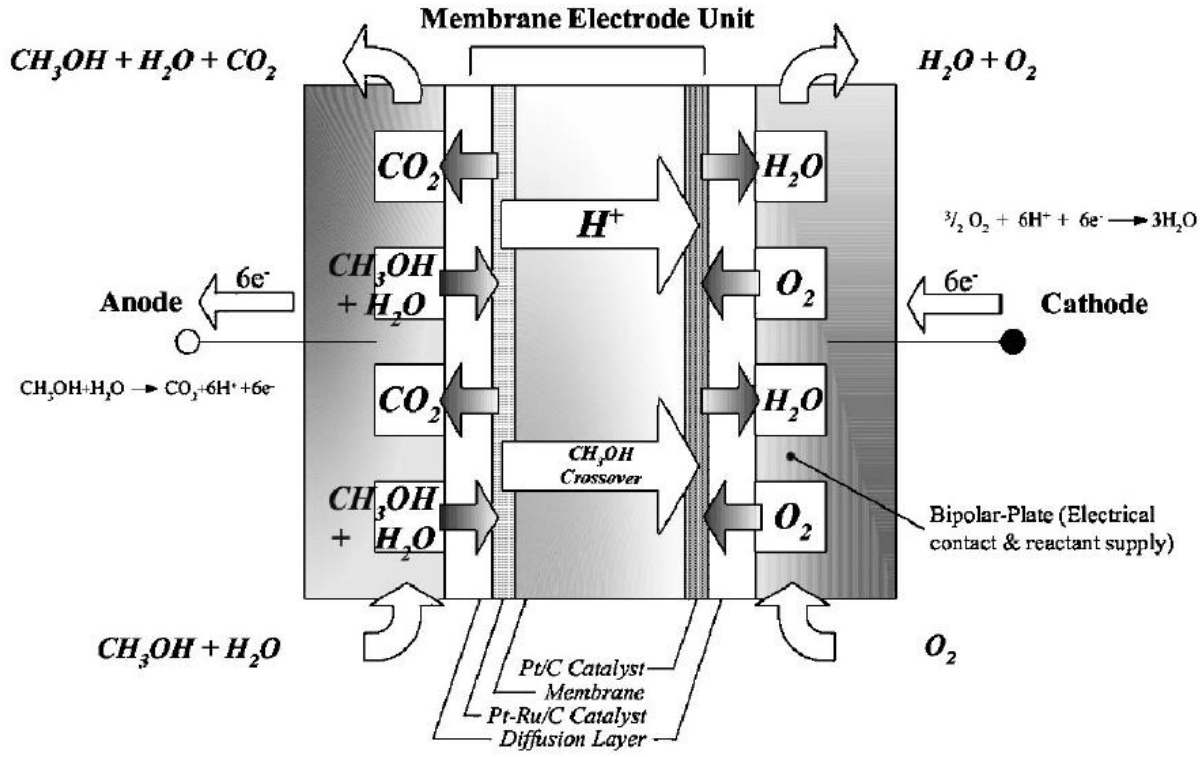

Figure 2.4 *Schematic diagram of a Direct Methanol Fuel Cell [39]*

2.2.2 CHALLENGES OF THE DIRECT METHANOL FUEL CELL

DMFC is available in the market, but there are some challenges that need to be addressed which will improve the commercialization and efficiency of this device. Construction and operational costs are one of crucial aspects on the successful development and commercialization of these fuel cells. To overcome the cost and improve efficiency and power density of these fuel cells various methods have been investigated. Ruey et al [36] developed a mini fuel cell stack for portable application using commercial MEAs with fabricated bipolar plates assembled into a 3.5 by 3.5 cm^2 stack. The completed mini DMFC stack had the maximum power density of 9.33mW/cm^2 which was similar to macro fuel cell stacks, proving the feasibility of micro-

electroforming bipolar plates for mini-DMFC stacks. Bac2 a UK-based global manufacturer and supplier of bipolar plates has developed a family of conductive composites called Electrophen that has been optimized for bipolar plates used in PEM and DMFC. The key benefits of Electrophen is its low cost and ease of moulding making scale up to mass production rapid hence reducing fuel cell stack cost and improving stack performance [40, 41, 42]

Research has been done on reducing the amount of noble metal catalyst loading without affecting the performance of the fuel cell [43].The overall performance of DMFC depends on a number of factors such as electrocatalytic activity of the anode, proton conducting membrane ionic conductivity and resistance to methanol crossover, and water management on the cathode electrode [44].Another drawback is the poor performance of the cathode electrode towards highly irreversible oxygen reduction reaction (ORR) and methanol crossover leading to potential losses causing reduction in efficiency. Oxygen reduction is an even more serious problem as this process is quite slow even on precious metal electrocatalysts and this limits the operation of these fuel cells [45-46].

In the study, properties of platinum nanoparticles dispersed on the CNT are monitored. The electrocatalysts will be reviewed for their methanol tolerance, activity and ORR. Nanoparticles are expected to poses different properties depending on their size and distribution on the support material.

2.2.3 METHANOL CROSS-OVER IN DMFCs

The performance of the direct methanol/oxygen fuel cell with proton conducting polymer electrolyte depends significantly on the conditions of electroreduction reaction. One of the

objectives of the membrane in PEM fuel cells is to prevent fuel from reaching the cathode side and undergo non-electrochemical oxidation. In DMFC the fuel tends to diffuse through the nafion membrane. Methanol interacts with the ion exchange sites and is dragged by hydronium ions in addition to diffusion as a result of concentration gradient between anode and cathode which result in short circuit of the whole fuel cell [47].

The methanol presence at the cathode decreases the available fuel cell voltage, also its oxidation at the cathode leads to lower fuel conversion efficiency in the form of lost fuel [48, 49]. The crossover reaction at the cathode is given by equation 2-2 below [50].

$$CH_3OH + 3/2O_2 \rightarrow CO_2 + 3H_2O \qquad \text{Equation: 2-2}$$

Methanol that crosses over to the cathode reacts directly with oxygen hence undergoing oxidation on the cathode at which oxygen reduction alone is intended to occur, resulting in mixed potential and decreased potential of the cathode (figure 2.5) [51].

Ramya and Dhathathreyan [52] measured the methanol flux rates across the nafion© membrane using cyclic voltammetry and chronoamperometry electrochemical techniques. They observed that the permeability increased with an increase in concentration of methanol and concluded that the optimum concentration of methanol would be 1-2M for operation in a fuel cell. Surampudi et al [53] also considered a DMFC working with liquid feed methanol at concentration range of 0.5-4.0M with varying temperature of 66-90 °C. A high DMFC performance was found at 250mA/cm^2 at 0.5V, 2.0 M methanol and a temperature of 88 °C . Lower voltages were observed with both high, (4 M) and lower (0.5 M) concentrations while higher voltages were obtained at 2.5M in the experiment performed by Jung H.D et al [54]. The lower performance at lower and

higher concentrations is due to concentration polarization and methanol crossover in both lower and higher concentrations respectively [55].

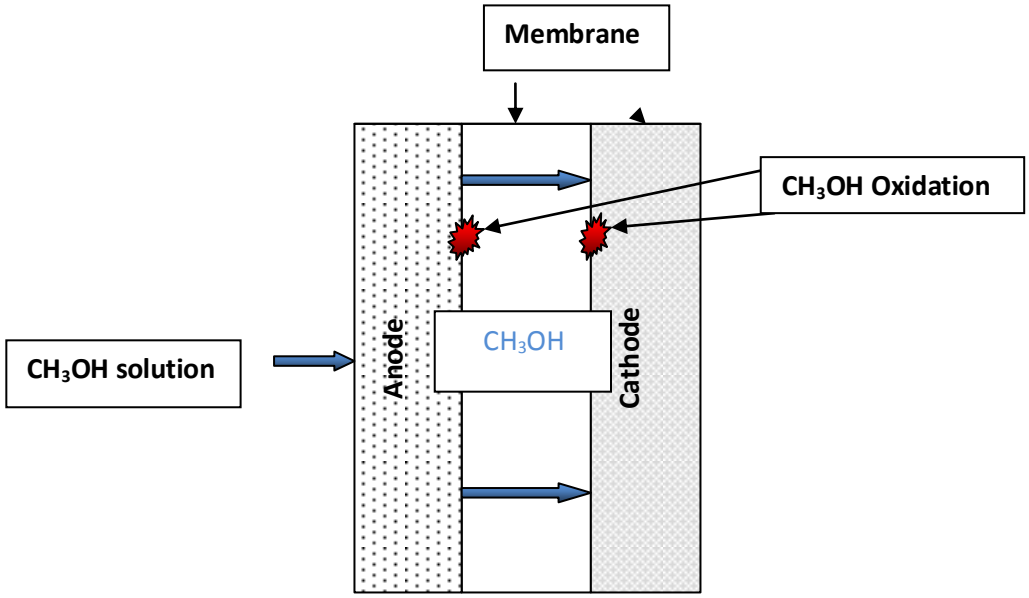

Figure.2.5 *Methanol crossover Phenomenon*

An increase of air flow produces better performances and it has been observed that the power generation is more significant in pressurized DMFC than operation at ambient pressure. A similar effect is produced by the cathode pressure. Methanol crossover is enhanced by the concentration and pressure gradient between the anode and cathode electrodes [14, 56].

This negative effect of methanol poisoning at the cathode can be limited by the use of relatively low methanol concentration in the anode feed solution and by increasing cathode pressure to a certain measure [57]. And also a compromise should be found for methanol concentration, it should be small enough to reduce crossover as much as possible but also supply the anode

catalytic layer with enough methanol to produce an acceptable current density. This draw back effect of the methanol crossover can then be minimized by the enhanced activity of the cathode catalyst, meaning that a Pt catalyst that can tolerate methanol poisoning is still needed for the cathode electrode.

2.3. ELECTROCATALYSTS

2.3.1 OVERVIEW OF ELECTROCATALYSTS

An electrocatalyst is a catalyst that participates in electrochemical reaction to modify and increase the rate of chemical reaction. They are a specific form of catalysts that can function either at electrode surfaces or as electrode surface itself. These materials enhance the electrode kinetics by minimizing the overpotential. The major applications of electrocatalysts are in water electrolysis, air batteries and importantly in oxygen reduction reactions and anodic oxidation of fuels in fuel cells [58]. Hence to make DMFC economically viable, it is imperative to minimize the overpotential losses by using appropriate electrocataysts.

2.3.2 ELECTROCATALYSTS IN DIRECT METHANOL FUEL CELL.

Both the anode and cathode electrodes of the DMFC need the employment of highly active electrocatalyst for the reactions required at these electrodes. Getting an insight from the electrochemical literature in the past years dealing with methanol oxidation and oxygen reduction, one can conceive two different trends. Investigations strive to find the basic understanding of the methanol oxidation and its mechanisms on different catalyst systems. The understanding of the oxygen reduction in the DMFC is another challenge that the researchers are

faced with. The effect of catalyst morphology and preparation on the catalytic efficiency may be another issue relevant to fuel cell researchers. The effect of particle size, surface area and the catalyst loading on the activity and efficiency of fuel cell is also one of the physical-chemical parameters that draw investigation interest. The catalyst requirements for a fuel cell are that, it must have high activity for the electro-oxidation of fuel at the anode and for the electro-reduction of oxygen molecule at the cathode electrode of the cell. Stability and good electric conductivity to minimize resistive losses on the catalytic layer is also required. The catalyst should also be less expensive in order to minimize the overall costs of the fuel cell [59]. Presently, platinum (Pt) and platinum based electrocatalysts are considered as the most active electrocatalyst for both electro-reduction of oxygen at the cathode and electro-oxidation of methanol at the anode [33]. The choice of platinum as electrocatalyst is due to the fact that it shows intermediate M-H adsorption energies and highest current, desorption occurs relatively faster hence the electrode surface is not easily poisoned by the adsorbed intermediates. Moreover Pt is stable in acidic medium even at relatively high anodic current and Pt is also readily available in various forms (plates, wires and powders).

2.3.2.1 DMFC Electro-oxidation

Electroactivity in direct methanol fuel cell anode electrode is one of the major challenges for this type of fuel cells because of the slow kinetics of methanol oxidation. The half cell reaction on this electrode is given by equation 2-3.

$$CH_3OH + H_2O \rightarrow CO_2 + 6H^+ + 6e^- \qquad \text{Equation: 2-3}$$

Platinum is a well known catalyst that has high activity for methanol oxidation and has been used for many years. However after some time, platinum gets poisoned by the adsorbed carboxylic species derived from the methanol oxidation. In order to solve this problem extensive research has been conducted using platinum based binary and ternary metallic electrocatalyst. The platinum ruthenium catalyst has been shown to be the best electrocatalyst for the direct methanol anode catalyst [60]. The electrooxidation mechanism in the direct methanol fuel cell needs to be understood as it is necessary for the optimization of this fuel cell. There is a generally accepted mechanism that occurs on the Pt based electrocatalyst and proceeds in several reaction steps. The first reaction is the adsorption of methanol on platinum which is immediately followed by its dissociation into several adsorbed species. In the next step the adsorbed species become more strongly adsorbed, accounting for the poisoning phenomena observed in this cell [61]. These reactions may be summarized as follows

$$Pt + (CH_3OH)_{sol} \rightarrow Pt\text{-}(CH_3OH)_{ads} \qquad \text{Equation: 2-4}$$

$$Pt\text{-}(CH_3OH)_{ads} \rightarrow Pt\text{-}(CH_2OH)_{ads} + H_{aq}^{+} + e^{-} \qquad \text{Equation: 2-5}$$

After some time the formyl-like $(CHO)_{ads}$ species are formed and become dissociated on the platinum catalyst surface which in turn results in strongly adsorbed carbon monoxide species, clearly identified as the poisoning species. This reaction is fast hence the poisoning is fairly rapid. The $(CHO)_{ads}$ species are then oxidized in the presence of OH molecules arising from the dissociation of water, leading to the formation of carbon dioxide molecules. Hence the reaction is as follows

$$Pt\text{-}(COOH)\ ads \rightarrow Pt + CO_2 + H^{+} + e^{-} \qquad \text{Equation: 2-6}$$

The presence of the catalyst in the anode electrode also facilitates the production of the hydrogen protons and electrons needed for the operation of the cell. The overall reaction of methanol conversion to carbon dioxide molecules and hydrogen protons on the anode of the fuel cell is

$$CH_3OH + H_2O \rightarrow CO_2 + 6H^+ + 6e^- \ (E_a = 0.02 \text{ versus SHE}) \quad \text{Equation: 2-7}$$

However after some time, platinum gets poisoned by the adsorbed carboxylic species derived from the methanol oxidation. In order to solve this problem, extensive research has been conducted using platinum based binary and ternary metallic electrocatalyst. The platinum ruthenium catalyst is currently accepted as the best electrocatalyst for the direct methanol anode catalyst [62].

2.3.2.2 DMFC Electro-reduction

Oxygen reduction occurs on the cathode electrode of the fuel cell. It takes place in the presence of a catalyst which speeds up the electrochemical reaction without it being used. The essential criteria for a better oxygen reduction electrocatalysts are: high electronic conductivity, chemical and structural stability under the operation conditions such as operating temperature, wide range of oxygen partial pressure and electrolyte concentration, ability to decompose the intermediate species formed during the reduction process, chemical and thermo-mechanical compatibility to electrolyte and interconnector materials, tolerant to contaminants and low cost [63, 64]. Methanol cross over is not completely preventable, small amounts are always available on the cathode electrode. To overcome the problems faced by the DMFC cathode, there is a need for the use of an active oxygen reduction electrocatalyst which is unaffected by the presence of traces of methanol or its oxidation products on the cathode. Platinum metal is used as electrocatalyst for

the oxygen reduction reaction in direct methanol fuel cells. Its electrochemical and chemical properties give it an advantage to be one of the best catalysts for this use. The kinetics of the ORR hinders the progress of the DMFC due to the sluggish reactions and the irreversibility of oxygen reduction reaction taking place on noble metals leading to extensive power density and efficiency loss of ~ 0.2V whereas methanol crossover is responsible for ~ 0.1V loss [65, 66]. The slow reaction rates are due to the high over-potentials associated with these metals. Two reaction pathways occur during oxygen reduction, the direct four electron route and the peroxide pathway. The direct four electron pathway is the more efficient in relation to the peroxide reaction because there is no peroxide species involved [39]. The reactions are summarized in Table 2.2. At first the oxygen molecules are adsorbed on the Pt surface, then dissociate and then hydrated to form Pt-hydroxide and Pt-oxide species. These species interact and combine by reduction with H^+ from the methanol oxidation to form water which is the byproduct of the fuel cell [67]. Hence the overall reaction for the four electron pathway in acid medium is as follows

$$O_2 + 4H^+ + 4e^- \rightarrow 2H_2O \qquad (E_c = 1.23V \text{ versus SHE}) \qquad \text{Equation: 2-8}$$

Table 2.2 Summary of reaction taking place on the cathode

	Acidic medium	**Basic medium**
Reaction	$O_2 + 2e^- + 2H^+ \rightarrow 2OH_{ads}$	$O_2 + 2e^- + 2H_2O \rightarrow 2OH_{ads} + 2OH^-$
Direct	$2OH_{ads} + 2H^+ + 2E^- \rightarrow 2H_2O$ Overall reaction $O_2 + 4H^+ + 4e_- \rightarrow 2H2O$	$2OH_{ads} + 2e^- \rightarrow 2OH^-$ Overall reaction $O_2 + 2H_2O + 4e^- \rightarrow 2OH^-$
Indirect	$O_2 + e^- + H^- \rightarrow HO_{2,ads}$ $HO_2 + e^- + H^+ \rightarrow H_2O$ Overall reaction $O_2 + 2H^+ + 2e^- \rightarrow H_2O_2$	$O_2 + H_2O + e^- \rightarrow HO_2 + OH^-$ $HO_{2,ads} + e^- \rightarrow HO2^-$ Overall reaction $O_2 + H_2O + 2e^- \rightarrow HO_2^- + OH^-$

Different schemes for ORR pathway have been proposed by different authors [68, 69, 70, 71, 72]. Of various schemes proposed for ORR, the scheme by Wrobla et al [70] appears to be appropriate to describe the reaction pathway for reduction of oxygen at the metal surface. In their mechanism they considered the adsorption – desorption steps of H_2O_2 at the electrode and developed a method to determine the mechanism of O_2 reduction.

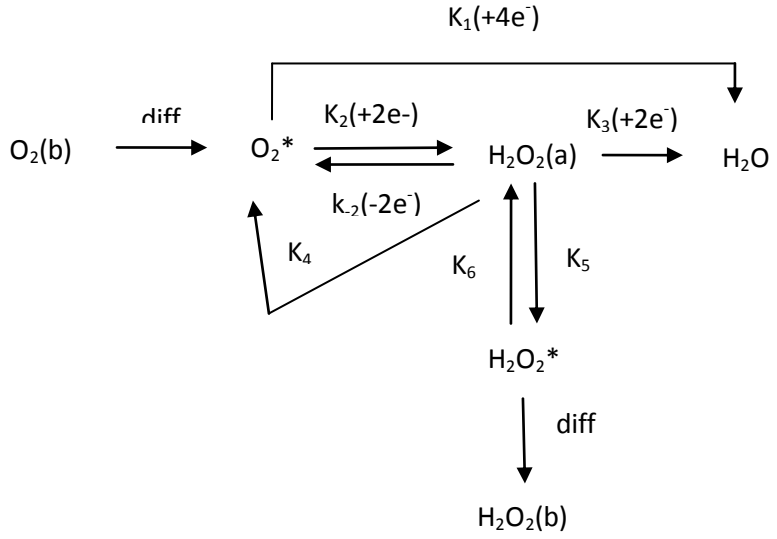

Figure 2.6 *Reaction mechanisms for oxygen reduction [70]*

However in the presence of methanol, pure platinum displays a formation of mixed potentials due to methanol crossover which leads to lower current densities and a decrease in the overall performance of the cell [73]. An approach in which pyrolyzed transition metal macrocycles are used as cathode catalysts, in the struggle against methanol crossover, have proven significant activities towards oxygen reduction. Out of these Fe and Co porphyrins and their derivatives appear to be the most active [74, 75]. The results obtained by Wang et al also proved that carbon

supported iron tetramethoxyphenyl morphyrin is methanol tolerant and an active catalyst for the oxygen reduction for a DMFC [76].

In recent years there has been a significant work done to reduce the platinum loading in DMFC electrodes. Methods of improving the activity and efficiency of this fuel cell include the use of binary catalysts and novel supporting material.

2.4 BINARY CATALYSTS AS ELECTROCATALYSTS FOR DMFC CATHODE ELECTRODE

The poisoning of the cathode catalyst (present due to methanol crossover phenomena) results in instability and reduced performance of the fuel cell. This problem may be solved by using electrolytes (i.e. Polymer membrane) with lower methanol permeability or by developing new cathode electrocatalysts with high methanol tolerance and higher activity for oxygen reduction than pure platinum. Developing a sufficiently selective and active electrocatalyst for DMFC cathode remains one of the key tasks for further progress of this technology. One of the routes being investigated is to test the activity of some Pt alloys towards oxygen reduction in the presence of methanol and use them as direct methanol fuel cell cathode catalysts [77, 78].

Platinum is the most active and stable catalyst that can electrolyze the oxygen reduction reaction (ORR) but is limited by the cost and hence there is a desire for the development of low or non platinum ORR catalysts. One method is to lower Pt content in the catalyst through alloying other low cost materials without compromising performance of the fuel cell [79]. The specific activity of Platinum bonded with other metals from the first transition (Cr, Fe, Ni, Cu, Co etc) is higher

than platinum alone. In these materials, the activity does not depend only on platinum but also on the nature of the second metal.

Tsivadze et al [80] saw these catalysts insufficiently tolerant to alcohols and modified them with phosphorus and sulfur to improve methanol tolerance. These electrocatalysts are termed modified binary catalysts. Their findings proved that Pt-Co-S/C is the most tolerant towards methanol than Pt-co/C and Pt/C electrocatalysts, its specific activity exceeded the other catalysts in the reduction reaction. The use of chalcogens, particularly sulfur for Pt/C modification results in an increase in methanol tolerance [81].

An investigation of bimetallic Pt-M/C as DMFC cathode catalysts by Baglio et al [82] shows that out of the three Pt-M (M = Cu, Co and Fe), Pt-Cu poses high degree of alloying although the same method was used for all three. It appeared that Pt-Fe catalyst was superior to other catalysts both in terms of catalytic activity and tolerance to methanol, also enhanced activity towards oxygen reduction reaction was improved. An improvement of the DMFC single cell performance was observed in the presence of Pt-Fe catalyst. According to Shukla et al and Xiong et al [78, 83] among the various alloy electrocatalysts investigated Pt-Co/C showed the higher catalytic activity for oxygen reduction reaction in relation to Pt/C. An enhanced electrocatalysis performance for the oxygen reduction reaction in the presence of methanol at Pt-Ni and Pt-Cr alloy electrocatalysts was observed [84, 85].

In contrast to other investigations some studies reveal that Pt-Cr system is less catalytic than pure platinum in any composition [86]. In the same way, Neto et al [87] observed that Pt-Co activity for ORR is lower than for pure platinum. However these investigations were carried out on

unsupported catalysts and on different conditions to those of the fuel cell. Thus, changes in the active area in gas diffusion electrodes and the cell operation conditions could explain the increased electroeactivity.

The improvement on the ORR electrocatalysis in these metal alloys has been ascribed to different factors such as changes in the Pt-Pt inter-atomic distance, surface area, d- orbital valency [88, 89] and also to the cell geometry. Furthermore this positive effect on the catalyst stability can be achieved by strengthening of the nanoparticle by supporting the metal catalyst on carbon. Several carbon supported binary catalyst have been shown to offer good performance as oxygen reduction catalysts for fuel cells with solid polymer electrolyte membrane. The strength is a result of adhesion or improved corrosion resistance of carbon surface regions adjacent to the metal nanoparticles. [80].

2.4.1 PARTICLE SIZE AND ALLOYING EFFECT OF Pt ELECTROCATALYST ON DMFC

Platinum electrocatalysts are dispersed as small particles on high surface area conductive supports for effective use of costly platinum. Therefore the size of platinum particles plays an important role in the oxygen reduction kinetics for fuel cell applications in terms of both electrocatalytic activity and practical application of the catalyst. Alloy catalysts with various transition elements were employed to increase the catalytic activity and reduce the cost, and Pt alloys have been reported to show higher activity than Pt alone. Many studies were conducted to identify the relationship between particle size and the oxygen reduction activity on Pt/C and Pt based electrocatalysts. The particle size effect on Pt/C has been well documented with some literature, however on alloy catalysts with transition metals, diverse results have been observed.

Beard and Ross [90] found that, with Pt-Co alloy system the specific activity decreased with an increase in surface area. Bregoli [91] also reached the same conclusion with his investigation. He found out that the oxygen reduction specific activity decreases with decreasing particle size between 12 and 2nm. On the other hand, Hwang [92] and Bett et al [93] observed a different effect that the specific activity was independent of the particle size. Hwang and Bett reached their suggestion experimenting with different catalysts, Pt-Fe/C and Pt/C (3 to 40nm) respectively. Yuan et al [46] came up with different suggestion, that higher net oxygen reduction and an increase in power densities of up to 20-30% was achieved on Pt-Fe/C than on Pt/C. This experiment was performed on half cells and on direct methanol fuel cell using voltammetric and steady state polarization measurements. They suggested that the increased activity of the alloy towards oxygen reduction was due to the larger active surface area of the alloy observed and also to the favored Pt-Pt distance.

In the investigation of some binary catalysts for enhanced oxygen reduction by Min et al [94], Pt and Pt alloy catalysts showed increased specific activity with decreasing surface area. In addition the Pt based alloy catalysts showed significant higher activities than Pt catalysts with the same surface area. This phenomenon comes from the reduced Pt-Pt neighboring distance and variations electronic states as the catalysts were alloyed. In this investigation Pt-Ni showed the shortest Pt-Pt distance and high activity. Therefore the particle size and alloying effect are two most important factors affecting the catalytic activity towards oxygen reduction. Supporting the catalyst with CNT increases the catalyst surface area and hence the activity of the catalyst.

2.5 SUPPORT MATERIAL FOR ELECTROCATALYSTS

The electrocatalytic activity can be enhanced by increasing the surface area through dispersion of catalysts on suitable support material and hence lowering the precious metal loading content. Some of the main properties required for practical supports that can be used with oxygen reduction electrocatalysts are:

- Acceptable electronic conductivity
- Adequate chemical or electrochemical stability in the electrolyte environment
- The ease of fabrication into electrode structures.

Carbon structures with surface areas ranging from less than $10m^2/g$ to over $1000m^2/g$ appear to pose many of these characteristics for oxygen reduction electrodes in fuel cells. Unfortunately, at high anodic potential these materials are susceptible to gradual electrochemical oxidation [95]. In past years carbon blacks were exclusively used as catalyst supports. To improve the electrochemical activity and stability of the catalyst, other carbon materials have been tested for their support qualities for fuel cell catalysts. These materials are in nanoscale range interms of their structural conformations, pore texture and their forms. Examples of these materials are carbon nanotubes (CNT), mesoporous carbons and microspheres [96]. Other support materials include calcium carbonate ($CaCO_3$) and metal oxides such as alumina (Al_2O_3), ziconia (ZrO_2) and silica (SiO_2). Carbon black and carbon nanotubes possess better support properties hence are considered as the best electrocatalyst supports [97].

2.5.1 CARBON BLACK

Carbon blacks, manufactured by pyrolysis of hydrocarbons such as natural gas or oil fraction from petroleum processing are widely used as catalyst supports [98]. Carbon black such as **Vulcan XC-72** is the most well known carbon support material due to its low cost, availability, high surface area with conventionally good conductivity, corrosion resistance and preferred pore size structure. The key structural deficiencies associated with carbon black are: broad pore size distribution with a significant portion being micropores with pore size < 2nm, low degree of graphitization and presence of surface functional groups [99]. With regard to support material, it was reported that the pretreatment of the carbon black before preparing the catalyst can enhance the catalytic performance. In recent studies the catalytic performance was related to the surface area of the supporting materials and to the size of the active metal. However there are problems associated with the carbon black, impurities which may poison and also deactivate the metal catalyst surface [100]. Some of these impurities were found to be Fe, Ca, Cl and S. unlike other supports like CNT the presence of such elements in carbon blacks affects the stability of the support hence of the supported catalyst [96].

2.5.2 CARBON NANOTUBES (CNT)

There are two common types of carbon nanotubes, single walled (SWCNT) carbon nanotubes, and multi walled (MWCNT) carbon nanotubes. Nanotube diameters ranges from approximately 0.4 to >3nm for SWCNT and from approximately 1.4 to at least 100nm for MWCNT.

(SWCNT) is a graphene sheet rolled into a cylindrical shape and a multiwalled consists of coaxially arranged graphene sheets rolled into a cylinder. The properties of nanotubes depend on atomic arrangement (how the sheets of graphite are rolled), the diameter and the length of the

tubes, and the morphology or nano structure. The atomic structure of nanotubes is described in terms of the chirality, which is defined by the chiral vector ($\mathbf{C}_h$), $C_h = n_{a1} + m_{a2}$, and the chiral angle (θ) as shown in Figure 2.7 below. Depending on the carbon bonds around the nanotube diameter, the nanotube is either of the armchair (n=m), zigzag (n=0 or m=0), or chiral variety. SWCNT may be metallic or semiconducting, depending on the sheet direction about which the graphite sheet is rolled to form a tube cilynder. This direction in the graphite sheet plane and the nanotube diameter are obtainable from a pair of integers (n, m) denoting the tube type [101, 102, 103].

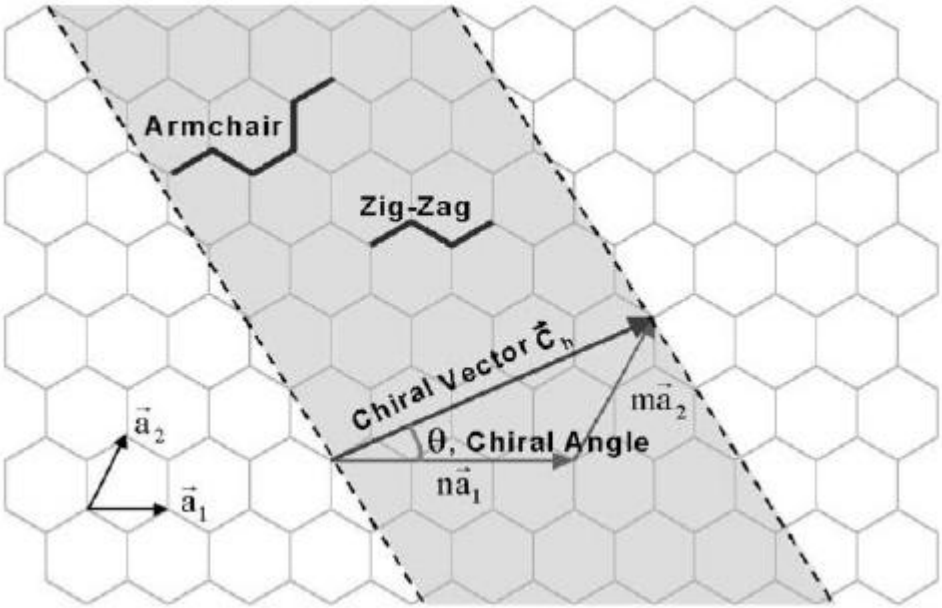

Figure 2.7. *Schematic diagram, showing how a hexagonal sheet of graphite is rolled to form a carbon nanotube [104].*

When viewed with transmission electron microscope (TEM) these tubes appear as planes. Whereas single wall nanotubes appear as two planes, in multi- wall nanotubes more than two planes are observed, and can be seen as a series of parallel lines. MWCNT can come in an even more complex array of forms, because each concentric graphene layer used to form MWCNTs can have different structures and orientations hence there are a variety of sequential arrangements. The simplest sequence is when concentric layers are identical but different in diameter. However, mixed variants are possible, consisting of two or more types of concentric tubes arranged in different orders. These can have regular or random layering. Their structure influences its properties including electrical and thermal conductivity, density and lattice structure. Both type and diameter are important. The wider the diameter of the tube, the more it behaves like graphite [105]. CNTs can be metallic or semiconducting depending on the structure and offers amazing possibilities to create future nanoelectronic devices. These materials have been investigated as advanced electrocatalyst support due to their distinctive electrochemical characteristics. CNT are made special by the combination of dimension, structure and topology that translates into a whole range of superior properties. The basic constitution of CNT is the C-C covalent bond which is one of the strongest in nature as in graphite. The perfect alignment of the lattice along the tube axis and the closed topology endows nanotubes with in-plane properties of graphite such as high conductivity, excellent strength and stiffness, chemical specificity, and inertness together with some unusual properties such as the electronic structure which is dependent on lattice helicity and elasticity [106].

Carbon nanotubes have attracted great interest from both a fundamental and applied point of view since their discovery by Iijima in 1991 [107, 108, 109]. These materials can be viewed as

tubular structures under electron microscope and are seen as the more appropriate candidates for oxygen reduction reactions owing to their outstanding mechanical characteristics such as high tensile strength coupled with nano-dimension providing high surface area, high electric conductivity and thermal conductivity [110]. However the distribution, deposition and size of Pt nanoparticles supported on CNTs depend on the surface functionalization of these materials. Furthermore; the electrocatalytic activity of Pt is also significantly affected by the nature of their interaction with CNTs and intrinsic properties of the carbon nanotubes [111,112]. Figure 2.8 shows a general structure of a MWCNT made out of different SWCNT.

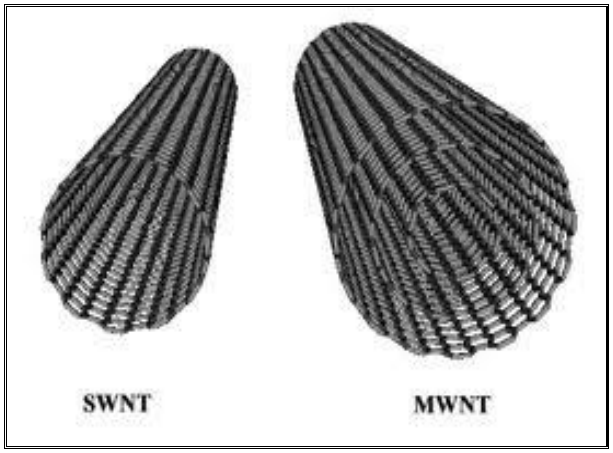

Figure 2.8 *Schematic diagram of single and multi walled carbon nanotubes.*

The application of carbon nanotubes as supports for platinum and platinum based alloy electrocatalysts on fuel cells has been reported [113, 114].

The platinum nanoparticles may be decorated on the surface of the CNTs by various methods such as: chemical reduction, electrochemical reduction, pyrolysis process. Among these methodologies, the one step electrochemical reduction is considered as an effective procedure for the preparation of Pt nanopaticles on carbon nanotubes when compared with other methods which are time consuming and where the impurities might be involved during the process [115].

2.5.3 SYNTHESIS METHODS FOR CARBON NANOTUBES

There has been extensive research on the synthesis of carbon nanotubes using such methods as arc discharge, laser vaporization and chemical vapor deposition. Among these methods, chemical vapor deposition of CNTs is said to be the best as it has many advantages such that CNTs can be synthesized with high purity, high yield, selective growth and vertical alignment [116].

2.5.3.1 Arc discharge method

Arc discharge was one of the first methods used to synthesize CNT on which a large research effort to find the best experimental condition is still on going in the scientific community. Although it is difficult to control the experimental device, arc discharge is mostly used for production of single wall carbon nanotubes. The electric arc discharge is generally performed in an evacuated reactor where after evacuation, a buffer gas like helium or hydrogen is introduced. The CNT can be formed during the condensation of carbon from two vaporized high purity graphite electrodes which are anode and cathode. The anode is then consumed by the voltage applied forming an arc and a constant gap between the electrodes is maintained by adjusting the position of anode. The material then deposits on the cathode [117].

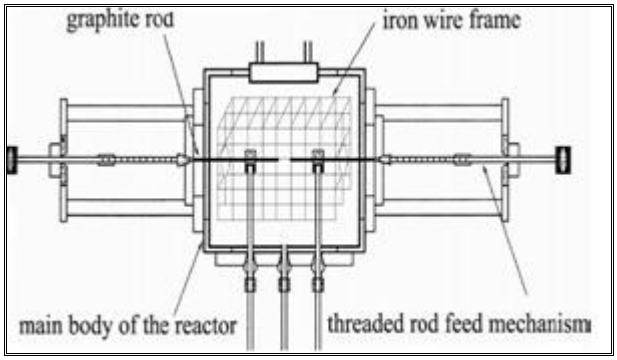

Figure 2.9 *Arc Discharge Schematic Diagram [118]*

.

2.5.3.2 Laser ablation

In this technique a laser is used to vaporize a graphite target held in a controlled atmosphere oven at temperatures near 1200° C. to produce CNT, the graphite target is coated with a metal catalyst. The condensed material is then cooled on a water cooled target [104]. A schematic diagram of laser ablation technique is shown in Figure 2.9.

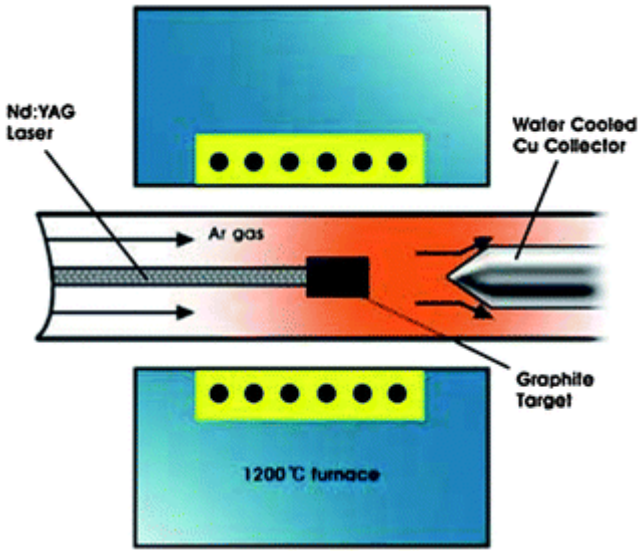

Figure2.10. *Schematic diagram of laser ablation technique [119]*

The arc discharge and laser vaporization techniques can produce the large amount of CNT depending on the size of the carbon source (anode in arc discharge and the target in laser ablation), but it is very difficult to control the alignment and size of the tubes. These techniques also require extensive purification process to separate pure CNT from other particles and very high temperatures are required (>2000) to vaporize graphite for CNT growth [119, 120].

2.5.3.3 Chemical Vapor Deposition (CVD)

CVD method is the most promising method to commercialize CNT growth due to the advantages in terms of its low cost, high yield and easy control. In this method, the quality of CNT growth depends on a number of parameters, including the catalyst type and composition, growth temperature, carbon source and gas flow rate. The active catalyst for CNT growth contains transition metal such as Fe, Co, Ni, Cr and others [121]. The CVD growth of CNT is accomplished by introducing a carbon source to the reaction chamber in the presence of a suitable metal catalyst and the chamber conditions have to be capable of decomposing the carbon source [122]. The growth mechanism involves simultaneous decomposition of a carbon source with a metal catalyst in a heated tube under inert atmosphere [123] followed by the dissolution of the carbon phase into metal catalytic nanoparticles and redeposition of carbon on the catalyst surface [103, 124].

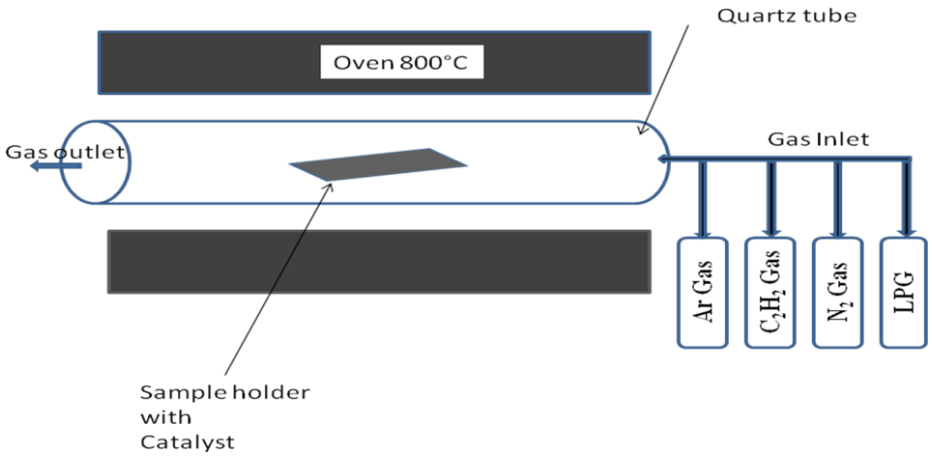

***Figure2.11**. Schematic of the furnace for chemical vapor deposition method [103]*

2.6 PREPARATION METHODS FOR SUPPORTED PLATINUM ELECTROCATALYSTS

Since the dispersion and particle size of Pt on the support material can strongly affect its utilization and catalytic activity, the synthesis of Pt/CNTs is of practical fundamental and practical importance. Several methods, well developed for Pt/C have been employed for preparation of Pt/CNT. These methods mainly include impregnation, precipitation, colloidal and ion exchange methods [125]. Figure 2.11 show some different deposition methods of Pt dispersion onto CNT.

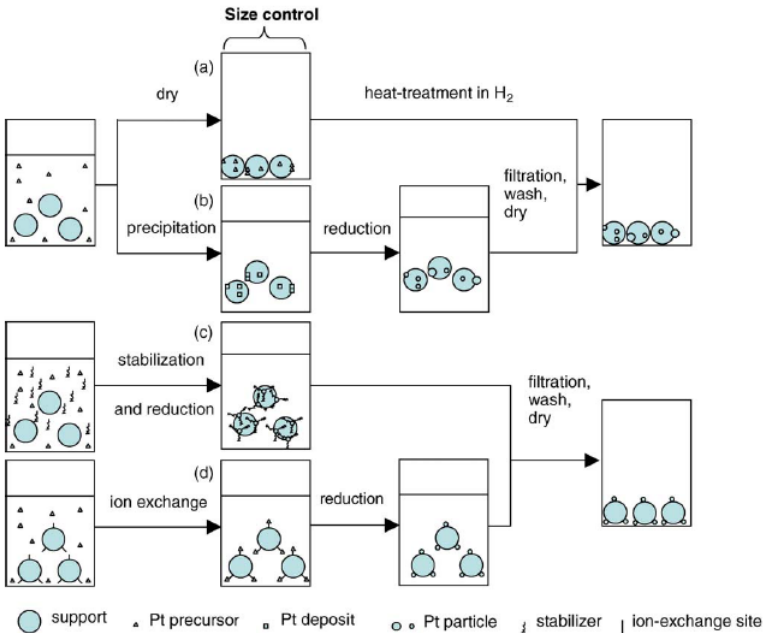

Figure 2.12 *Schematic illustrations of (a) Impregnation, (b) precipitation, (c) colloidal and ion exchange [125].*

2.7 SUMMARY

DMFC are believed to be one of the best options for low temperature fuel cells for portable and stationary applications. To improve the use and commercialization of the DMFC in the market, it is necessary to reduce the cost. The major cost with this type of fuel cell is due to the expensive platinum used as the catalyst at the anode and cathode electrodes. In order to reduce the cost, optimum utilization of Pt with small particle size evenly dispersed with high electrochemical activity must be achieved. Physical properties of the carbon support can greatly affect the electrochemical properties of the electrocatalyst. The amount of Pt used also needs to be reduced. To use small amounts of platinum support materials with high surface area, conductivity, and good crystallinity, chemical and mechanical properties must be used.

Although many attempts have been made to overcome methanol crossover in DMFC, it still remains a challenge affecting the use and overall performance of these fuel cells. Electrocatalysts with small particle sizes offer a high electrochemical activity. Carbon nanotube supported Pt have been investigated for the cathode electrode of the DMFC, to minimize this phenomenon. Physical-chemical properties of cathode electrocatalyst, including metal particle size, distribution and dispersion, crystallinity, morphology and electrochemical active area is critical.

3. EXPERIMENTAL WORK

This chapter provides detailed descriptions of the methods, materials and techniques that were used to characterize the electrocatalysts (synthesized or commercial) used in this study. The physical – chemical properties of the electrocatalyst play a vital role in enhancing the performance of the catalyst and cost reduction. The literature has revealed that the decreased particle size of an electrocatalyst lead to a change in the properties. Upon decreasing the particle size and uniformly dispersing the nanoparticles on the supporting material the activity of the catalyst is increased and the amount of the catalyst use is minimized, hence the cost reduction and enhanced performance of the fuel cell. Pt nanoparticles can be dispersed as small particles when the support material is conductive and have high surface area. For this reason it becomes crucial to understand and measure the enhanced properties of these materials as their characteristics play a very important role for application as catalyst for DMFC.

In this study, platinum nanoparticle electrocatalysts are dispersed on the surface of a conductive support material for effective use. The preparation methods and techniques used to analyse the Pt/C and Pt/CNT nanomaterials are discussed. Sample preparation methods and other experimental parameters are also described.

As discussed in the literature review section, the following techniques have proven to be useful and will be used as techniques in the investigation of the electrocatalysts prepared.

For structural Identification of the catalysts three instruments were used.

Scanning electron microscopy (SEM), Transmission electron microscopy (TEM), X-ray diffraction spectroscopy (XRD)

For elemental analysis

Energy Dispersive X-ray Analysis, (EDS)

For electrochemical characterization

Cyclic voltammetory (CV), Scanning electrochemical microscopy (SECM)

In the sections below, materials used are tabulated and brief description on the various instrumentation, principles, operation conditions and the way in which these techniques were applied in characterization of the electrocatalysts are presented.

3.1 MATERIAL AND METHODS

3.1.1 Materials and Chemicals used

The materials used in the study are tabulated in **Table 3.1** and the chemicals used in the preparation of the solutions are shown **Table 3.2**. In **Table 3.3** a list of instruments used for charactorisation.

Table 3.1 Materials Used in Synthesis or Testing

Material	**Supplier**	**Purpose**
Commercial 20% Pt/C	BASF	Electrocatalyst for baseline studies
Carbon nanotubes	Synthesized in the lab	Support for Pt Nanoparticles
Commercial carbon nanotbes	BASF	Support for Pt Nanoparticles
Carbon black	Carbot	Gas Diffusion layer
(AB_5) $LaCeNi_5$	Gaungzhou research institute for non ferrous metals (China)	Catalyst for CVD synthesis of CNT
PTFE (Teflon®)		Binder for GDL

Table 3.2 Chemicals used for catalyst preparation.

Chemical	**Supplier**
Chloroplatinic acid $H_2cl_6.6H_2O$	Alfa easer
1-Propanol ($CH_3CH_2CH_2OH$)	KIMIX
Nafion solution	Ion Power, Inc
H_2SO_4 (98%)	KIMIX

NHO_3 (55%)	KIMIX
Formaldehyde	KIMIX
HCl (32%)	KIMIX
KOH	KIMIX
Ethylene glycol (99%)	Sigma Aldrich

Table 3.3 Instruments used

Technique	**Information given by the technique**
Gas phase chemisorptions	Metal surface area and dispersion
X-ray Diffraction (XRD)	Metal crystallite size, metal lattice parameter
Scanning Electron Microscopy (SEM)	Morphology, Elemental composition
Transmission Electron Microscopy (TEM)	Particle size, distribution , Morphology
Atomic Absorption Microscopy	Morphology of CNT
Energy Dispersive Spectroscopy (EDS)	Elemental composition
Particle Induced X-ray Emission (PXE)	Elemental composition, dispersion and distribution
Electrochemical Scanning Microscopy (SECM)	Surface activity/topography
Cyclic Voltammetry (CV)	Electrochemical Surface activity

Other equipment used

- Bendelin Sonoex Sonicating bath
- Prona Spray gun
- Puncher
- Labofan Tube Furnace
- Binder Oven

3.1.2 PREPARATION OF SOLUTIONS

Chloroplatinic acid preparation

Two separate solutions of chloroplatinic acid were prepared using ethylene glycol and isopropanol as solvents. A required amount of chloroplatinic acid was weighed and transferred to a 50ml beaker. This reddish brown powder was then dissolved in a known volume of ethylene glycol or isopropanol. A 0.5M solution of chloroplatinic acid was obtained.

Synthesis of Carbon Nanotubes (CNT) and Subsequent Treatments

3.1.3 SYNTHESIS OF CARBON NANOTUBES

Multi-walled carbon nanotubes (CNT) were prepared using chemical vapor deposition method (C VD) adopted from Ndungu et al [126].

Two sets of CNT were produced by this method using different hydrocarbon gases, ethylene and Liquid petroleum gas (LPG) as carbon source.

(i) Synthesis of CNT using LPG as a carbon source

Carbon nanotubes were grown on an AB_5 ($LaCeNi_5$) group intermetalic compound catalyst. 1g of the catalyst was placed on an alumina boat and the boat was then loaded and centered in the quartz tube located inside the horizontally aligned tube furnace. The quartz tube was then sealed with appropriate gas fittings for the delivery and removal of the gases. A flow of nitrogen was initiated (flow rate = 40ml/min) to remove air in the quartz tube. After 10 minutes, the furnace temperature was increased to 800℃ at a heating rate of 24℃/min, once the temperature had stabilized at 800℃, the nitrogen flow was stopped and the LPG flow initiated at a flow rate of 40ml/min. after 60 minutes, the furnace was switched off and a flow of nitrogen at 20ml/min was started again to provide an inert atmosphere preventing oxidation of the carbon nanotubes while the tube cools down to room temperature. 6g of CNT were produced. In this study these CNT are referred to as LPGCNT.

(ii) Synthesis of CNT using ethylene as carbon source

The same procedure as for the LPGCNT synthesis was followed during the production of these CNT using pretreated catalyst, ethylene as carbon source and argon gas to remove the air and provide inert atmosphere in the tube. The catalyst ($LaCeNi_5$) was treated by heating and stirring 5g of $LaCeNi_5$ in 50ml 0.2 M HCl at 50℃ for 30 minutes. 1g of the purified catalyst was use for production of CNT and the same procedure as of the LPG CNT was followed. The CNT were

then removed from the furnace and stored for further use. Approximately 5.3g of CNT were produced. CNT produced were termed ECNT.

3.1.3.1 Treatment of synthesized carbon nanotubes

To improve the catalyst loading and uniform nanoparticle dispersion and size distribution of the catalyst for better activity and efficiency of the electrocatalyst the support material needs to be contaminant free. Produced carbon nanotubes (0.6g) were treated to remove the impurities that may have been formed and the excess catalyst particles left during the synthesis process and to introduce functional groups (carboxylic, hydroxyl) that serve as anchors that promote platinum deposition on the surface of the CNT. Carbon nanotubes produced were treated with nitric acid and then treated with mixture of nitric acid and sulfuric acid to purify and also introduce functional groups on the CNT. In a round bottom flask (200ml) containing CNT, 100ml of a 40 and 60ml of 8M H_2SO_4 and NHO_3 respectively, was added in each flask. The flask was then put onto an ultrasonic water bath for 30 minutes at room temperature and then refluxed under air at 120 °C for 3hours. The mixture was left to cool to room temperature and washed with ultrapure water until the pH was around 6-7. The CNT were dried overnight at 100° in a vacuum oven. The mass of the CNT after treatment was 0.48g.

3.1.3.2 Deposition of platinum on carbon nanotubes

Platinum nanoparticles were deposited on both LPGCNT and ethylene CNT. This was achieved by reducing a platinum salt precursor, chloroplatinic acid hexahydrate ($H_2PtCl_6.6H_2O$) in

Ethylene Glycol. This method is similar to the one used by Yangchuan Xing [127]. Multi-walled carbon nanotubes were placed in a 100ml glass flask, a 45ml volume of ethylene glycol was added and 5ml of 0.05M $H_2PtCl_6.6H_2O$ solution in ethylene glycol was added. The mixture was subjected to agitation in a sonic bath at room temperature for 20minutes then magnetically stirred under reflux between 110 and 130℃ for 15 hours. After 5 hours of stirring, 2ml of 0.4MKOH was added. The platinum loaded carbon nanotubes were then separated from the ethylene glycol by vacuum filtration and washed with ultrapure water. The catalyst was dried in a vacuum oven overnight at 80°C. Platinum supported on CNT (PT/MWCNT) were obtained and ready to be characterized for physical and electrochemical properties.

To investigate the effect of different solvents in the deposition of nanoparticles on the support, isopropanol was also used for Pt deposition on CNT following the same procedure and formaldehyde as a reducing agent.

3.1.3.3 Electrode preparation

Pt/CNT (25mg) was placed in a glass vial, 50mg water and 75mg of 5% nafion© solution was added. A small amount of isopropanol was added. The mixture was then sonicated at room temperature for 30 minutes.10ml isopropanol was added and sonication continued for 2 hours. The mixture was then mechanically stirred for another 2 hours. The ink was sprayed on a 4x2cm^2carbon paper with a gas diffusion layer (GDL) to obtain a 0.25 mg/cm^2 catalyst loading using a spray gun. The GDL was prepared the same procedure as the ink using desired amount of carbon black and PTFE instead of catalyst and nafion©.

3.2 PHYSICAL CHARACTERIZATION OF ELECTROCATALYSTS AND SUPPORT MATERIAL

3.2.1 SCANNING ELECTRON MICROSCOPY (SEM)

Scanning electron microscopy is an imaging technique used in all fields that require characterization of solid materials, with the ability of producing profiles of material surfaces. It permits the observation and characterization of heterogeneous organic and inorganic materials on a nanometer (nm) to a micrometer (μm) scale. SEM is easy to operate, with user friendly intuitive interfaces and minimal sample preparation. SEM is used to provide information about the surface morphology, particle size and appearance of supporting material and electrocatalysts. This instrument is also used to identify phases based on quantitative and qualitative chemical analysis.

The fundamental operation of this instrument involves the acceleration of electrons carrying a significant amount of energy, and the energy is dissipated as a variety of signals produced by the electron-sample interactions when the incident electrons are decelerated in the solid sample. The signal derived from the electron-sample interactions reveal information about the sample including external morphology, chemical composition and orientation of the materials making up the sample. The magnification of an SEM image is governed by the differences between dimensions of the video display and that of the area scanned on the specimen surface. Increased magnification is achieved by scanning smaller areas on the specimen [128, 129]

3.2.1.1 Sample preparation

SEM does not require much sample preparation as it is used for solid samples and powders. The samples for analysis in the SEM must be appropriate size to fit in the specimen chamber and mounted tightly on the sample holder. Conventional SEM requires that a sample be electrically conductive on the surface to prevent the accumulation of the electrostatic charge. For non-conducting samples this can be overcome by covering a sample with a thin layer of conducting material such as gold or platinum and other conductive coating materials [129, 130]

SEM samples were prepared by placing a double sided conductive carbon tape on the stub. A small amount of the sample was deposited on the stub, then shaken and gently tapped to remove the excess and loose sample. The stub was then mounted on the SEM sample holder and. All specimen were conductive, no coating was required. The samples were then inserted in the vacuum chamber of the microscope for analysis. In this study a Nano Nova SEM was used, the parameters are listed in **Table 3.4** below.

Table 3.4. SEM parameters.

Parameter	**Setting**
Working distance	15mm
Accelerating voltage	25keV
Tilt Angle	0°

Aperture	0.4mm
Resolution	3nm

3.2.2 TRANSMISSION ELECTRON MICROSCOPY

The transmission electron microscopy (TEM) is conventionally used to characterize the microstructure of materials with spatial resolution providing information about the morphology, crystal structure and defects, crystal phases and composition, and magnetic microstructure can be obtained by a combination of electron-optical imaging (2.5Å point resolution), electron diffraction, and small probe capabilities. The diverse range of structural information and high resolution is the challenge of producing very thin samples for electron transmission.

3.2.2.1 Sample preparation for TEM Analysis

Sample preparation for TEM generally requires more time than for most other characterization techniques. A TEM specimen must be approximately 1000A or less in thickness in the area of interest. In this study,TEM is used to elucidate metal nanoparticle size, particle size distribution, homogeneity and agglomeration of the supported electrocatalyst. The metal surface area can be obtained from TEM data by using an equation 3.1 below

$$SA_{Pt} = 6x\ 10^3/ (d\ \rho) \qquad \text{Equation 3-1}$$

Where d = density of Pt (21.4g/cm^3) and ρ = particle size in nanometers (nm).

Specimens were prepared by dispersing a small amount of the sample in about 5ml of methanol, followed by agitation in a sonic bath for 10 to 15 minutes. A drop of the suspension was deposited on the copper coated carbon or formvar® mesh with a diameter of about 3mm. the sample was then left at room temperature for methanol to evaporate and then placed on the sample holder and introduced directly in the shaft for analysis. All prepared samples were viewed and photographed using a Tecnai G^2 F20X Twin Mat electron microscope. The experimental parameters are given in the **Table 3.5** below.

Table 3.5 Tecnai G^2 TEM operational parameters.

Parameter	**Settings**
Accelerating voltage	200kv
Current	20 μA
Condenser aperture	1
Objective aperture	3
Exposure time	3s

3.2.3 X-RAY DIFFRACTOMETRY

X-ray diffraction is a rapid technique that gives information about the structure of the solid materials, the arrangement of atoms that compose the solid sample and crystallinity of the

sample. It is widely used because of it permits nondestructive structure characterization and is extensively used acquire qualitative, quantitative, crystallinity, residual stress and crystallite size information of solid samples. In this study XRD is used to investigate the atomic structure, particle size and lattice parameter of the electrocatalysts and the support material. The metal surface area of the Pt catalyst (SA_{Pt}) can also be determined using particle size obtained from XRD data. SA_{Pt} is calculated using equation 3-1 given above as presented by Prabhuram et al [131].

During sample analysis in the X-ray diffractometer, the crystalline solid sample is bombarded with X-ray beam which causes crystal plane atoms to diffract X-rays in various angles. These X-rays are generated by the cathode ray tube, filtered to produce monochromatic radiation, collimated to concentrate and directed towards the sample. When the X-ray beam hits the atom of the sample, the electrons around the atom start to oscillate with the same frequency as the incoming beam and there will be well defined X-rays beams leaving the sample at various directions (constructive interference) if the conditions satisfy the Brag's law given by equation 3-2 below, which relates the wavelength of electromagnetic radiation to diffraction angle and the lattice spacing in a crystalline sample.

$$n\lambda = 2d\sin\theta \qquad \text{Equation: 3-2}$$

All possible diffraction directions are attained by scanning the sample through a range of 2θ angles, due to the random orientation of powder samples [132].

The degree of crystallinity of the sample can be measured by the width of the peak in a diffraction pattern associated with a particular planer reflection from within the crystal unit cell. The larger the peak area the more amorphous the sample is and if the area under the peak is narrow, the sample is more crystalline. XRD can also be used quantitatively to elucidate the particle size using the Scherrer equation, given as:

$$D = 0.9\lambda / \beta\cos\theta \qquad \text{Equation: 3-3}$$

Where D = particle size, 0,9 =shape factor, λ = x-ray wave length, β =peak –width at half-height (radians), θ = angle of reflection.

In addition to the information provided, the lattice parameter (α) can be calculated by the following equation:

$$a_0 = d\,(h^2 + k^2 + l^2)^{1/2} \qquad \text{Equation: 3-4}$$

Where *h*, *k*, and *l* constitute the Miller indices of a crystal facet, and *d* is the interplanar spacing determined using Braggs' Law.

XRD analysis was done at iThemba Labs, diffractograms were recorded using Bruker AXS D8 Advance measurements X-ray diffractometer. The specifications are listed in Table 3.6 below

Table 3.6 XRD, Bruker AXS D8 specifications

Parameter	**Condition**
Tube	Copper
Detector	Lynx-Eye position sensitive detector
Monochromator	None
Generation operation	40kV and 40mA
Current	40mA
X-ray source	CuK_{α} (λ= 1.5418 Å)

3.2.4 NITRGEN ADSORPTION AT 77K

The surface area of the catalyst is an important parameter in catalytic processes that controls the performance of various components and determines the reaction rate. For quality control purposes, the rapid determination of surface area and average particle size are required. Several methods are available for evaluating surface area, but most attention focuses upon gas adsorption methods such as that used by Brunauer, Emmett and Teller (BET) based on the isothermal adsorption of nitrogen [133]. The BET theory is based on the phenomenon of physical adsorption of gases on the external and internal surfaces of porous material. Such materials, surrounded by and in equilibrium with a gas, which has a certain temperature T and relative

pressure, p/p_0 adsorbs physically a certain amount of gas. The amount of the adsorbed gas is dependent on its relative vapor pressure and is proportional to the total internal and external surface of the material. The connection between vapor pressure and amount of adsorbed gas at constant temperature is called an adsorption isotherm [134]. The surface area and porosity of the supports and electrocatalysts were determined using a Micromeritics Acceleration Surface area and porosity ASAP® 2020 Accelerated Surface Area and Porosimetry Analyzer system. Pore size, pore volume and pore size distribution of the samples can be obtained using the Barrett-Joyner-Halenda (BJH) method.

3.2.4.1 Sample preparation

Prior to analysis, the samples were placed in an oven at 80°C for overnight to remove any form of water that may be present. A small amount (approximately 0.06g) was transferred into a sample tube and subjected to degassing at 150°C for 30 minutes. The tube was then sealed and inserted into the analysis port and analyzed at liquid nitrogen temperature (-196°C).

3.2.5 ATOMIC FORCE MICROSCOPY (AFM)

Atomic Force Microscopy is one of the families of scanning probe microscopes which has grown steadily since the invention of the scanning tunneling microscope (STM) and is a very high-resolution type, with demonstrated resolution of fractions of nanometers, more than 1000 times better than the optical diffraction limit. In this technique, a fine tip is brought into atomically close contact with a sample surface without actually touching the surface. This is done by sensing the repulsive force between the probe tip and the surface. The forces are extremely small

(about 1 nano-Newton) and these forces depend, in part, on the nature of the sample, the distance between the probe and sample, the probe geometry, and any contamination on the sample surface . The tip is then moved back and forth over the sample surface and can measure the topography with almost atomic resolution. This technique is also capable of manipulating molecules and measuring the strength of molecular interactions with pico-Newton sensitivity. AFM provides a profile of the surface on a nano-scale, by measuring forces between a sharp probe (<10 nm) and surface at very short distance (0.2-10 nm probe-sample separation). The AFM can be operated in different modes depending on the nature of the application. Generally, possible imaging modes are divided into static and dynamic modes depending on the net forces between the probe and the sample [135].

In a dynamic mode (non-contact) the AFM is operating in the attractive region, where the AFM cantilever is curved toward the sample, since it is being pulled by attractive forces. The probe is pulled toward the surface primarily by capillary forces on contaminated samples and Van der Waals forces on clean samples. Operation in the repulsive region is called static (contact) imaging, and the cantilever is curved away from the sample due to the repulsive forces [136].

In this investigation, atomic force microscopy from digital instruments (veeco metrology group) with scan magnification of up to 105X 105 μm and scan rate of 0.800 Hz was used for characterization of the support material. The sample line and aspect ratio used was 512 and 1.00 respectively for all the samples. A tapping mode was used as it is believed to be suitable for rough samples.

3.2.5.1 Sample preparation

Samples were prepared by sonication of as mall amount (spatula head) of sample in 5ml methanol in a sonic bath at room temperature for 30minutes then a dropped on a pretreated silicon wafer. The wafer was cleaned by sonicating it in acetone for few minutes and air dried before depositing the sample.

3.2.6 PROTON INDUCED X-RAY EMMISION

Proton induced x-ray emission (PIXE) is the highly sensitive, rapid and non-destructive multi-elemental qualitative and quantitative analysis technique. The proton induced x-ray emission has advantage among other instruments due to its large cross section for X-ray production and the background contribution is low. In PIXE analysis, the first part is to identify the atomic species in the target from the characteristic peak energies in the x-ray emission. This is followed by determination of the amount of a particular element present in the target from the intensity of the characteristic emission spectrum. Characteristic x-rays are emitted by a sample surface upon bombardment with accelerated protons originating from a nuclear microprobe and a particle accelerator. PIXE can be combined with other methods like Rutherford Back Scattering (RBS) and /or sample etching techniques to perform in depth profile analysis [137, 138]

The use of PIXE in this study is for mapping the surface elemental distribution of electrocatalysts.

3.2.6.1 Sample preparation

Samples were prepared by spraying the required amount of ink (electrocatalyst) on carbon carbon paper which was used as a substrate. The samples were aloud to dry in air. The samples were then mounted on a sample holder and loaded into the spectrometer. RBS analysis was also performed followed by the dynamic analysis of surface composition.

Table 3.7 PIXE analysis parameters

Parameter	**Conditions**
Scan	2.669 x2.669mm
Proton accelerating velocity	3MeV
Number of pixels	128 x128
X-ray analysis line	L-shell

3.3 **ELECTROCHEMICAL CHARACTERIZATION OF SUPPORTED ELECTROCATALYSTS**

3.3.1 SCANNING ELECTROCHEMICAL MICROSCOPY (SECM)

Scanning electrochemical microscopy is one of the Scanning Probe Microscopes (SPM) in which three – dimensional images of surfaces are obtained. This process involves scanning a small ultra microelectrode (UME) tip across a surface (substrate) and recording an appropriate response. The size of the UME tip makes them ideal for rapid voltammetric measurements due to their

small ohmic drop and double layer capacitance. SECM differs from other SPM techniques by its high spatial resolution, its ability to image surfaces of various kinds and its applicability to quantitative measurements through well developed fairly rigorous theory. The SECM response depends on the rate of mass transfer of target species to UME tip positioned in a solution (phase1) in a close proximity to the second phase which may be solid liquid or gas. The mass transfer rate in turn is governed by physic-chemical processes at the part of the interface directly under the tip. Studies of this technique also include the use of the equilibrium perturbation mode to probe molecular and ion transfer processes and feedback mode to measure the rate of interfacial redox reaction.

The imaging in the SECM experiments are classified as either feedback or generation collection (GC) at which the feedback mode is the most commonly used. In the feedback mode, the ultra-micro electrode tip current is perturbed from its value in bulk solution by the presence of a much larger substrate at close proximity. If an oxidizing species in the solution is reduced at the UME tip and the substrate is conductive and held at sufficiently positive potential, the tip generated reduced species is oxidized and the tip current is increased. This process is termed positive feedback. A negative feedback occurs at non-conductive or insulating of the substrate where no oxidation occurs and the tip current decreases [139, 140].

To study the electro-conductivity of membranes or cast films, the approach curves are conducted prior to imaging. The approach curves are used when generation of a reduced species occurs at a limited rate. In this mode, the tip of a UME is positioned at a certain distance above the

substrate, as the distance between the tip and the substrate decreases the regeneration of the reduced species is fast enough thus the current increases. Using the well-developed quantitative theory for each situation, one can simulate tip-current against distance curves with the help of computers [141]. In this study SECM is used in qualitative characterization of electrocatalysts for their topography and surface activity [142, 143].

Studies of the electrocatalyst topography were done using a Uniscan Instruments SECM 270. The samples were prepared by dropping approximately 2µl of the electrocatalyst ink on HOPG which was then dried in an oven at 80℃ for 10 to 15 minutes. The sample was then placed in a cell. 0.01M H_2SO_4 was used as electrolyte, Pt wire as counter electrode and Ag/AgCl reference. Two working electrode were the tip probe (ultra-microelectrode) and the eectrocatalyst electrode.

Ultra-micro electrode was fabricated by sealing a 2cm Pt wire with a diameter of 25µm in a capillary tube. The tube was then heated to fuse the wire with the tube. The end of the tube was then polished producing a fine tip with exposed disk. Before characterization of the sample, the UME was first investigated for its performance in 0.01M potassium ferricyanide and 0.1 potassium chloride as the supporting electrolyte, at a sweep rate of 50mV/s.

3.3.2 CYCLIC VOLTAMMETRY

Cyclic voltammetry (CV) is popular for its powerful investigation of the electrochemical behaviours of a system. The CV makes possible the elucidation of the kinetics of electrochemical reactions taking place at electrode surfaces. It is possible to investigate the role of adsorption, diffusion, and homogeneous chemical reaction mechanisms from the sweep rate, width and

potentials of the peaks observed in the voltammogram. It offers a rapid determination of redox potentials of electroactive species [145].

Cyclic voltammetry plays an intergral part in a comprehensive characterization of nanophase electrocatalysts. CV is currently widely employed in structural, as well as electrocatalytic activity characterization of electrocatalysts. CV can also be used for determining the electrochemical active surface area of supported nanoelectrocatalysts.

Cyclic Voltammetry, in this study was used to elucidate the electrochemical activity of the electrocatalysts at room temperature using the Autolab PGSTAT 30 (parameters are given on Table 3.8). The experiments were conducted in a three electrode cell with a gas diffusion electrode as a working electrode. The platinum basket and Ag/AgCl were used as counter and reference electrodes respectively. 0.5M H_2SO_4 was used as the electrolyte in all the experiments. Prior to the measurements the working electrode potential was cycled for 20 cycles between -0.2 and 1V vs. Ag/AgCl at 50mVs^{-1} scan rate to remove all contaminants that may be on the electrode surface and to obtain a stable cyclic voltammogram. Before scanning, the electrolyte solution was purged with nitrogen for an hour to remove dissolved oxygen. For oxygen reduction reaction experiments the electrolyte was bubbled with oxygen for 30 min and after that the electrode was purged with oxygen while the experiment was running. Then the electrode was screened between 1 and -0.2 V at 20mVs^{-1}. This technique was also used to study the behaviour of the electrocatalysts in the presence of methanol. Different concentration of methanol was added into the cell to monitor which of these electrocatalysts tolerated better the poisoning. All the gases used were from Afrox Company.

Table 3.8 Auto Lab CV parameters.

Parameter	Conditions
Voltametric assemble (AUTO LAB)	Metrohm (Eco Chemie BV, Netherlands)
Woking electrode	Gass diffusion electrode (Pt)
Reference electrode	Silver/silver chloride (Ag/AgCl)
Counter electrode	Platinum wire basket

4. CHARACTERIZATION OF SUPPORT MATERIALS AND SUPPORTED ELECTROCATALYSTS

4.1 STRUCTURAL CHARACTERIZATION OF THE SUPPORT MATERIAL

This section presents the characterization and interpretation of results for the support material. Carbon nanotubes synthesized by chemical vapor deposition method were characterized using various techniques. The results in this section start with morphological characterization of synthesized CNT using optical microscopy such as, scanning electron microscopy (SEM), transition electron microscopy (TEM) and atomic force (AFM) followed by crystallinity and graphitization characterization by XRD. The surface area and pore size of the tubes was also investigated by BET analysis. Commercial CNT were also characterized for use as reference.

4.1.1 SEM characterization of CNT

Carbon nanotubes synthesized by CVD method were characterized using SEM. Two sets of CNT were synthesized using different gases as carbon source (LPG and Ethylene) as discussed in section 3.3.1 above. Figure 4.1 shows the SEM image of CNT. CNT produced using LPG are termed LPGCNT and ethylene produced are named ECNT.

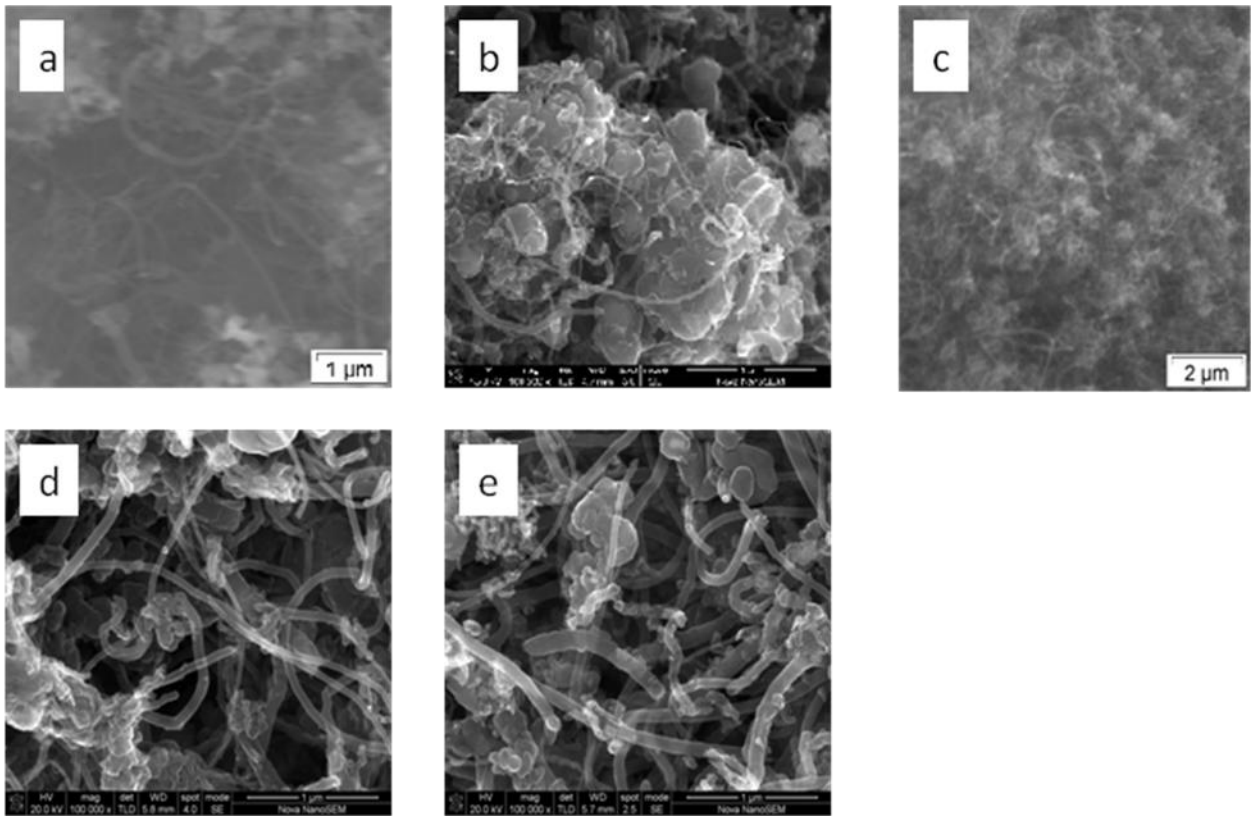

Figure 4.1 *SEM images of CNT, (a) LPG CNT, (b) ECNT and (c) commercial MWCNT. Acid treated (d) ECNT and (e) LPGCNT.*

The SEM micrographs show tubular like structures with varying degrees of curvature, and interspersed irregular shaped objects that maybe amorphous carbon or catalyst particles. The SEM images are typically what is reported in the literature for CNT [110]. Due to the nature of the sample in the images it is difficult to say with certainty where the CNT begins and ends, but an estimate of 30-60 micrometers, diameters of 10 different tubes were measured and the average diameter was 50. When comparing CNT before and after treatment Figure 4.1 (b) and (e) respectively, there is less amount of the irregular shaped objects showing that some of the amorphous carbon and other material such as catalyst residues have been removed by the acid

treatment. To confirm the absence or presence of catalyst on CNT, EDS was employed. The CNT after treatment appear to be broken, thus the length is shortened and the ends are open. SEM confirms the presence of carbon nanotube but does not distinguish which type of CNT was formed.

4.1.2 Energy Dispersion spectroscopy study of CNT

EDS was used to measure the amount of elements present in synthesized CNT and the weight percentages are given in Table 4.1

Table 4.1 EDS composition of synthesized CNT

Sample Name		Wt. % of elements before treatment			Wt. % of elements after treatment			
	C	¤ Ni	La	O	C	Ni	O	
LPGCNT	65	0.95	2.4	-	94.05	0.43	5.51	
ECNT	83.96	10.78	4.88	-	91.55	0.47	7.97	

The EDS results show that CNT are composed mostly of carbon and prove that the treatment process helped to eliminate the catalyst residue but small amounts of nickel are still observed. Lanthanum was not detected after acid purification and cerium was not detected even before the purification. This is because, Ce dissolved in HCl during the treatment of the catalyst prior to carbon nanotube production. The presence of oxygen on treated CNT is due to the introduction

of surface oxygen containing groups, such as carbonyls, during treatment with acids which helps enhance the deposition of catalyst on CNT.

4.1.3 Transmission Electron Microscope analysis

TEM was used to analyze the shape and diameter of the synthesized CNT. TEM technique can also observe the presence of amorphous carbon and residual catalyst particles.

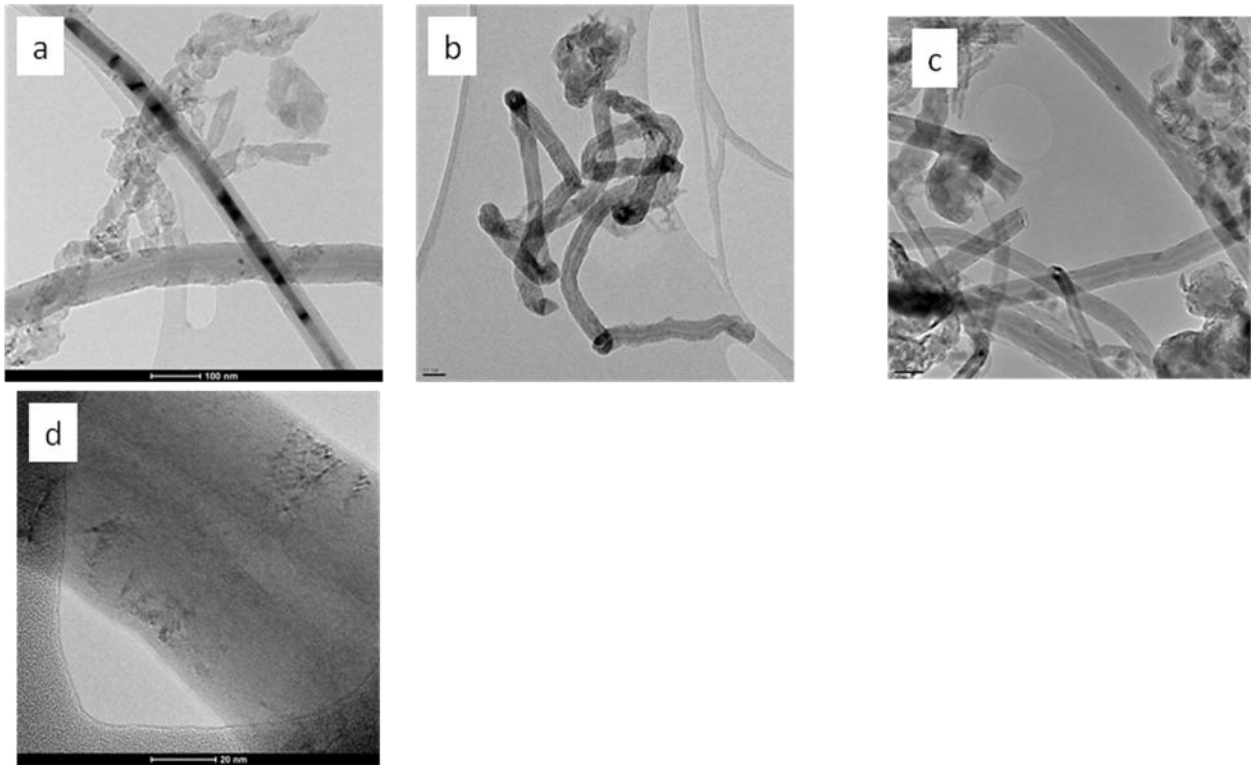

Figure 4.2 *TEM images of untreated LPGCNT (a), treated (b)ECNT,(c) LPGCNT and (d)HRTEM of LPGCNT.*

Typical TEM images of CNT are shown in figure 3. TEM image (figure 3a) shows CNT before treatment and shows that with some CNT the catalyst residues are trapped inside or at the tips of the tubes. This result highlights the mixed nature of the growth of the mechanism of the CNT

with the CVD process used. The general mechanism for CNT starts with the decomposition of carbon source on the metal catalyst, followed by diffusion and saturation of carbon into the catalyst, and then precipitation of the carbon as cylindrical structures [146]. Depending on the interaction between metal and support, the CNT can grow from the tip or base of the metal particle [147]. Location of metal particles on the tip of the CNT in the images shown favor tip growth mechanism, and the incorporation of the metal in the CNT one may speculate growth of CNT from opposite ends of metal particle, resulting in the trapping of metal in the CNT.

After treatment (figure 3b and c), it was found difficult to locate metal particles at the tips of the CNT indicating the removal of a significant amount of the metal catalyst and the open ends of the CNT can be seen. Figure 3d shows the structural defects caused by the treatment process on the walls of the CNT and the number of layers proves that the CNT produced by CVD are multi-wall which is in agreement with the literature. The diameter s of the CNT from TEM images was found to be 16-76 nm for LPG and 21-85 nm for ECNT and summarized in table 4.2 below.

Table 4.2 Diameter of CNT from TEM analysis

CNT	Inside diameter (nm)	Outside diameter (nm)
LPGCNT	6-14	16-76
ECNT	7-21	21-89
Commercial CNT	3-7	10.3-27

The TEM images show that nanotubes have been broken down to smaller pieces. This means that the aggressive acid treatment can digest [148]. Although treating the CNT with acid mixture is an effective method to remove impurities and catalyst residues, there are some serious disadvantages observed such as severe breaking and damaging of the walls. This will significantly impact physical – chemical properties of the CNT, such as mechanical and transport properties, chemical and electrical characteristics and will result in low yield because most CNT would be digested [149].

4.1.4 X-ray Diffraction analysis

In order to confirm the SEM and TEM results and to know the crystallinity of the synthesized CNT, XRD analysis was employed.

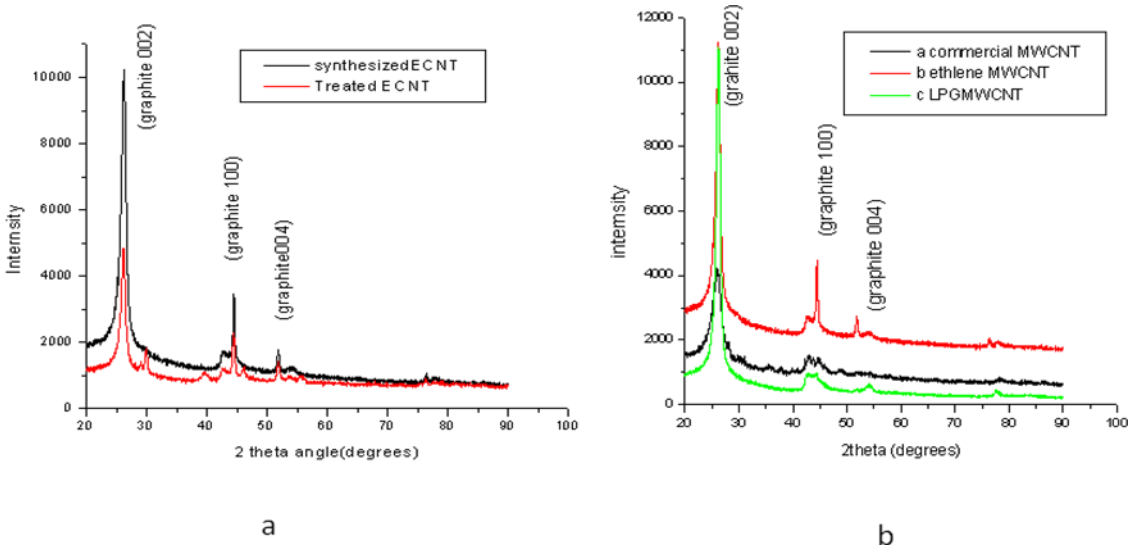

Figure 4.3 *XRD results of (a) untreated and treated ECNT (b) treated CNT.*

The XRD results in Figure 4.1.3(a) show diffraction peaks observed at 2θ = 26.31, 44,0 and 55° 2θ which can be attributed to the hexagonal graphite structure peaks 002, 100 and 004 of the multi-walled carbon nanotube [150]. After treatment with the acid, the graphitic intensity of 002 peaks increased mixture (XRD analysis done under the same set of conditions) and may be due to the removal of the amorphous carbon and highlights the crystallinity of the CNT. The crystallinity of the CNT from figure 4.1.3 (b) is in the order of LPGCNT > ECNT > Commercial CNT. The synthesized CNT are distinctly crystalline compared to the commercial CNT. Thus they are expected to poses higher electronic conductivity than the commercial. The interplanar spacing of the all CNT at 002 is 3.38Å. The calculated d-spacing is close to the d spacing of an ideal graphite crystal which is 3.35Å [151].

4.1.5 Surface area analysis of the support material

The surface area of the synthesized CNT was investigated by the BET method using nitrogen as adsorbate as described in section 3.3.4. The N_2 adsorption is known as a method to determine the pore size, pore volume and specific surface area of the porous materials. The pore size and surface area are summarized in table 4.1.3 below.

Table 4.3 Surface area and pore size of MWCNT

Sample	BET Surface area (m^2/g)	BJH Pore size (Å)	Pore volume (cm^3/g)	Micro Pore area (m^2/g)	Diameter range (nm)
Untreated MWCNT					
LPGCNT	81.4706	174.334	0.242088	7.0461	16-79
ECNT	29.8617	515.328	0.096210	0.7658	21-85
Commercial CNT	143.0422	185.122	0.695149	4.8056	10-27
Treated					

MWCNT					
LPGCNT	78.5993	149.216	0.215975	1.9377	10-50
ECNT	50.9425	170.564	0.140912	4.1551	18-64
Commercial CNT	189.0295	191.706	0.674227	10.6227	7-22

The surface characterization of the multi-walled carbon nanotubes by N_2 adsorption shows that the surface area and the pore volume of the MWCNT increases with decreasing diameter observed from the TEM micrographs with ECNT having the smallest surface area. The surface area increases significantly after the acid of treatment ECNT and commercial CNT. Nui et al [152] observed that the electrical conductivity of CNT can be enhanced by functionalization. This is due to the reduction or complete removal of the impurities and catalyst residues. Commercial CNT have the highest surface area, pore size, and pore volume and micro-pore area before and after the acid treatment. The minimal change in the textural properties of LPGCNT is inline with the XRD results. The LPGCNT showed more crystallinity (from the XRD) and were expected to be the list affected by the acid treatment and thus less change seen in the BET and BJH data. However ECNT and commercial CNT were both dramatically affected by the acid treatment with 70% and 32% increasing surface area respectively. The more crystalline a CNT sample is, the more it is resistant towards chemical attach [153,154]. This does not follow the crystallinity trend, and may be ascribed to the differences in the CNT samples in terms of average lengths, diameters, and curvatures and kinks (defect sites) present in the CNT, making it difficult to compare these two specific samples.

4.1.6 Atomic force analysis of MCNT

Atomic force microscopy (AFM) has been used extensively in the characterization of functionalized carbon nanotubes [155]. The AFM images were obtained using the taping mode in air. The scanning probe was a monocrystalline silicone cantilever with an integrated conical shape Si tip. In Figure 4.4 below are the MWCNT images.

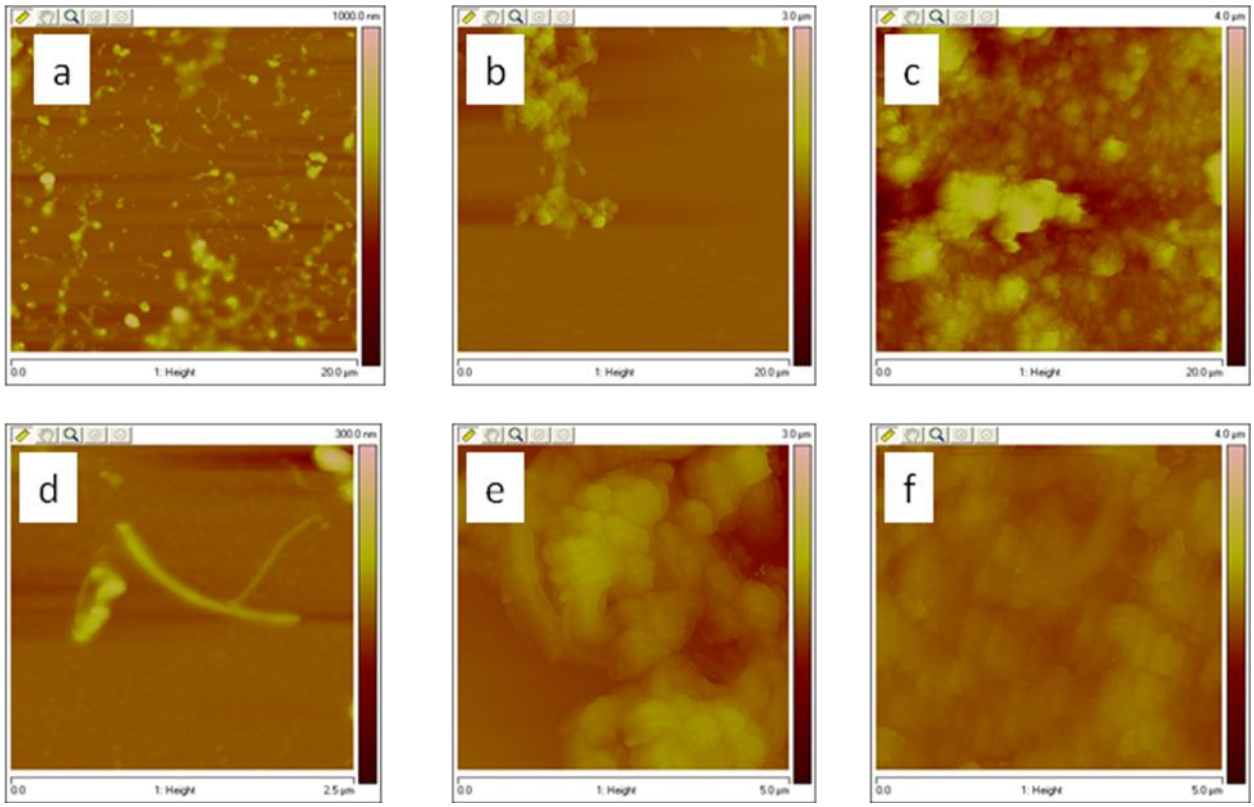

Figure 4.4 *AFM images of treated MWCNT (a) ECNT, (b) LPGCNT and (c) commercial CNT at 20µm scan range. Lower scan range images (d), (e) and (f) for ECNT, LPGCNT and Commercial CNT respectively are also shown.*

Figure 4.4 (a)-(c) above shows that the purified CNT contain little puffy round objects. This shows that some contaminants and byproducts from production are still present which is in agreement with the TEM and SEM results for treated CNT. Images (e-f) are taken at lower scan rate and prove that the surface of MWCNT becomes cleaner and purer after treatment, a large number of metal catalyst and amorphous carbon and other impurities have been removed. The carbon nanotube average diameter obtained from the ECNT image (e) measured using Nanoscope 7.30 software was 50nm which is within the range observed by TEM. LPGCNT and commercial CNT were shortened as observed in TEM micrographs and are close to each other making it difficult to measure the diameter using the Nanoscope software. The roughness factor of the CNT increased after treatment. This may be due to the introduction of the functional groups and etching of the outer surface of the tubes by the acid mixture, which enhances in anchoring the catalyst nanoparticles on the surface of the CNT.

4.1.7 Summary

From this study it is evident that the best method for detailed analysis of carbon nanotubes is TEM. Due to the high resolution of TEM, the sample can be observed even at atomic resolution. The carbon nanotube diameter was observed by TEM. Atomic force microscopy can also observe the presence of CNT and impurities, however it is time consuming compared to other methods and the diameter of the tubes could not be measured in all samples due to the poor resolution. AFM and SEM are good for the information about the over all morphology of the sample.

SEM characterization of the CVD produced CNT confirmed that a considerable amount of the CVD product was carbon nanotubes. Amorphous carbon and catalyst residue was also observed and confirmed by TEM. LPGCNT and ECNT produced have tube diameters of up to 75 and 85nm respectively. TEM, SEM and AFM proved that the acid mixture can be an efficient solvent for the purification of CNT but small catalyst residues were left behind as proved by the EDS analysis. The commercial CNT showed higher surface area of 143 and 189m^2/g before and after purification. The large surface area of the support can provide the necessary three-phase zone for electrocatalysis, which includes the reactant gas, solid catalyst surface and ions from the electrolyte, and the electrical pathways for efficient distribution [156]. LPGCNT showed less change in surface area after purification which is attributed to high crystallinity of the sample XRD results display the peaks of CNT identical to those of an ideal graphite sample. This confirms the graphitic structure and characteristics of carbon nanotubes.

4.2 CHARACTERISATION OF PLATINUM ELECTROCATALYST SUPPORTED ON MULTI-WALL CARBON NANOTUBES

Structural and electrochemical characterization of synthesized supported platinum nanoparticles is investigated in this section. The study was initiated by physical characterization of synthesized Pt/CNT and commercial Pt/C that can be potentially used as electrocatalyst of the cathode electrode of a DMFC. The investigation is followed by the electrochemical characterization of the electrocatalysts. The methods used for characterization of these electrocatalysts are discussed in chapter 3.

4.2.1 STRUCTURAL CHARACTERIZATION OF ELECTROCATALYSTS

Structural characterization of the supported electrocatalyst was conducted using a range of powerful techniques.XRD, SEM, EDS and TEM were used in the characterization process. Synthesized platinum supported on CNT was characterized, using the commercial Pt/C as the reference.

4.2.1.1 Particle size and crystallinity of the supported electrocatalysts

The particle size and crystallinity of the electrocatalysts (Pt/ECNT, Pt/LPGCNT and Pt/C) were determined using the XRD technique. Powder X-ray diffraction patterns of the synthesized and commercial electro-catalysts recorded at 2θ range of 10° to 90° are shown in figure 4.5

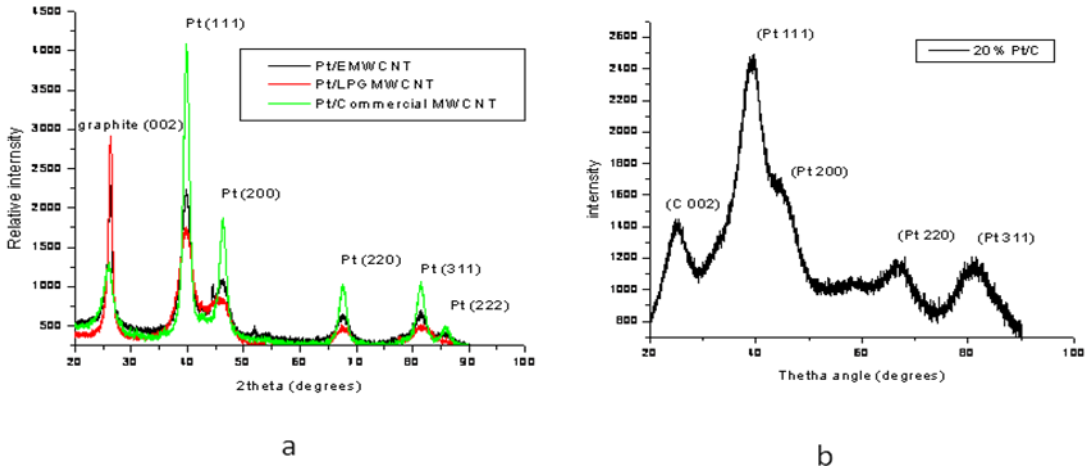

Figure 4.5 *XRD patterns of (a) synthesized Pt/ MWCNT and (b) commercial Pt/C*

The diffraction patterns for Pt/MWCNT exhibited five diffraction peaks at 2θ angle = 39.76°, 46.35°, 67.55°, 81.45° and 85.90° corresponding to the (111), (200), (220), (311) and (222) Pt

planes respectively. Electrocatalysts prepared with isopropanol as the solvent were also characterized and poses a similar pattern and the shown in **Appendix A**. Figure 4.2 (b) is a commercial Pt/C showing corresponding peaks to those of Pt/MWCNT except the absence of the (222) peak. The Pt/C diffraction shows broader diffraction peaks of Pt which is believed to be indicative of increase in nano-sized particles or amorphous nature of Pt particles and their good interaction with the support. The intensity of the peaks in Figure 4.2 (a) is narrow, suggesting more crystalline particles. The peaks at (002) are graphite or hexagonal structure of carbon support.

The d-spacing and particle size of Pt/MWCNT was calculated from LPGMWCNT as all the samples showed same Pt peaks at the same 2θ values and Pt/C were calculated from Bragg's Law ($n\lambda = 2d\sin\theta$) and Scherrer equation ($D = 0{,}9\lambda/\beta\cos\theta$) respectively. Lattice parameter was also calculated from the following equation3.4: $a_0 = d\sqrt{(h^2 + k^2 + l^2)}$ also given on chapter 3.

Calculated particle size, d-spacing and lattice parameter are summarized in Table 4.4 below.

Table 4.4 Particle size, Lattice parameter and d-spacing of electrocatalysts.

Pt/LPGCNT					**Pt/C**				
FCC facet	2θ	d2θ (Å)	D (Å)	a_o	FCC facet	2θ	d2θ	D (Å)	a_o
111	39.76	2.25	2.25	3.89	111	39.51	2.28	2.23	3.94
200	46.35	1.98	2.25	3.96	200	46.11	1.97	2.23	3.94
220	67.55	1.38	2.25	3.90	220	67.30	1.39	2.23	3.93
311	81.45	1.18	2.25	3.91	311	81.21	1.18	2.23	3.91
222	85.91	1.13	2.25	3.91	-	-	-	-	-

The diffraction peaks exhibited by Pt/MWCNT and Pt/C are similar to those observed by Praburam et al [157] and are indicative of the presence of Pt in face centered cubic structure. The lattice parameters are in good agreement with the crystallographic directions calculated as 3.9Å at (111) and (200) in observations reported on the review by Kim et al [158]. The interplanar spacing of the Pt electrocatalyst is in agreement with the findings by Oishi K and Savadogo O [159]. Surface area (m^2/g) was also calculated from the XRD data using the following equation:

$$S=6x10^3/\rho d$$

Where S = surface area (m^2/g), ρ = Pt density ($21.4g/cm^3$) and d = average particle size (nm).The surface area was found to be $124m^2/g$ for Pt/MCNT (which is a collective for all MWCNT supported Pt) and $125.7m^2/g$ for Pt/C.

4.2.2 MORPHOLOGY AND ELEMENTAL ANALYSIS OF SUPPORTED ELECTROCATALYSTS (Pt/MWCNT)

Morphology and elemental analysis of multi-walled carbon nanotube supported Pt electrocatalyst was conducted by SEM and EDS following procedures given in chapter 3 section 3. Figure 4.6 below shows SEM micrographs of Pt/MWCNT, the weight percentages of the loaded platinum are given in Table 4.5 EDS spectrum are shown in **Appendix B**.

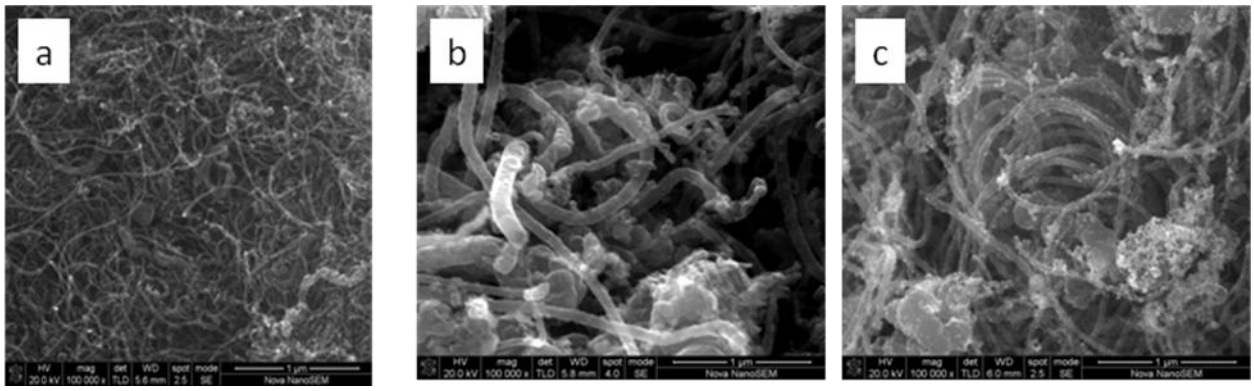

Figure 4.6 *SEM images of Pt/MWCNT (a) Pt/commercial CNT, (b) Pt/LPGMWCNT and (c) Pt/EMWCNT*

Table 4.5 Pt wt% on carbon nanotube supported catalysts.

Pt/MWCNT	Wt%
Pt/EMWCNT	21.8
Pt/LPGMWCNT	19.10
Pt/commercial MWCNT	16.74

In all the images shown in Figure 4.6 above, the particles of platinum appear to be dispersed on MWCNT. Pt nano- clusters are also observed on the walls of the MWCNT. The EDS analysis shows that a percentage loading of about 20% Pt was achieved in Pt/EMWCNT and Pt/LPGMWCNT as expected. Pt loading on commercial CNT was small. Particle size measurements could not be conducted using SEM due to the magnification of the SEM (100K), thus limiting the SEM to morphology and distribution in this study.

4.2.3 PARTICLE SIZE AND MORPHOLOGY FROM TEM

TEM analysis was employed to study the metal particle size of the synthesized electrocatalysts supported on Carbon nanotubes. Characterization was conducted on Pt/MWCNT including the ones prepared using isopropanol as solvent. Pt/C was also analyzed for comparison. The images for TEM analysis are shown in Figure 4.7 below.

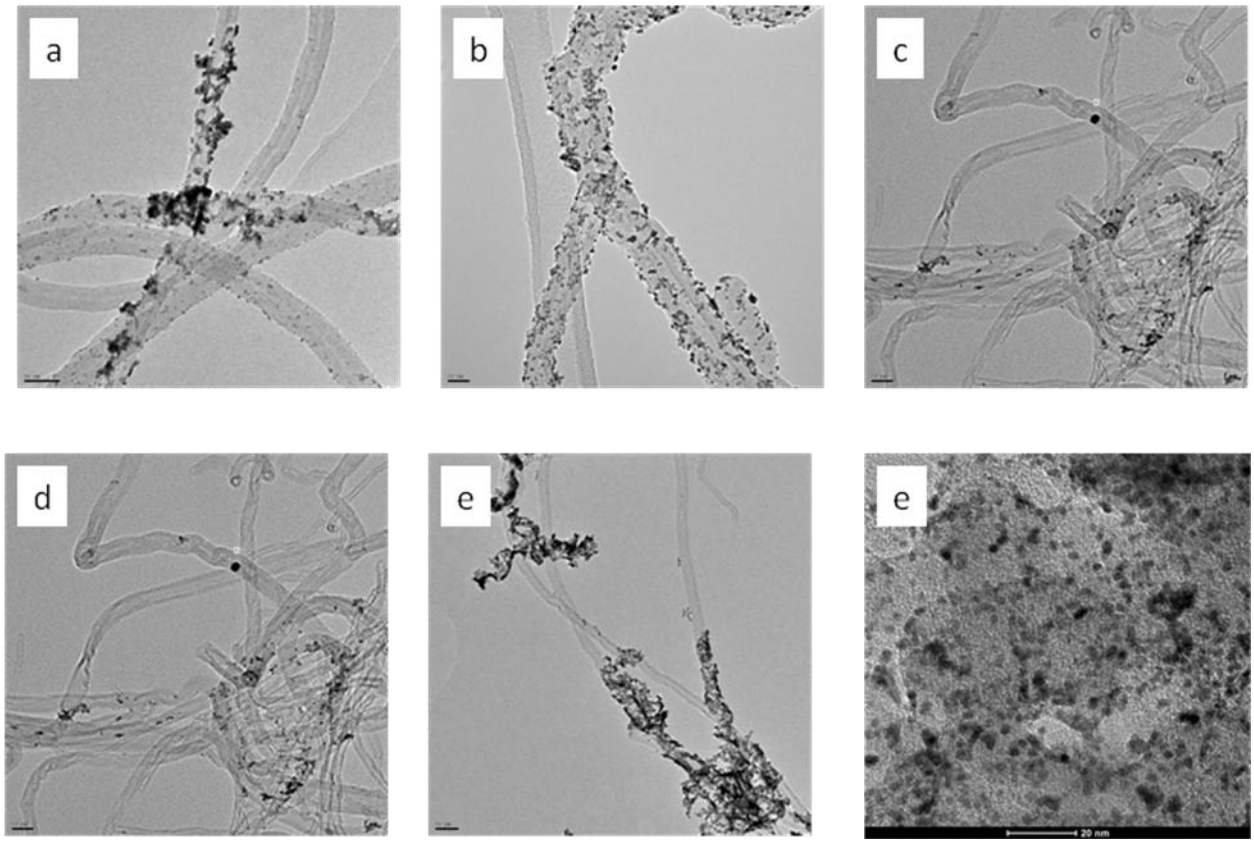

Figure 4.7 TEM micrographs for (a) Pt/EMWCNT, (b) Pt/LPGMWCNT, (c) Pt/commercial CNT. (e) and (f) are Pt/EMWCNT and Pt/commercial CNT prepared using isopropanol as solvent. (f) Pt/C

The TEM images (figure 4.7 a and b) show well dispersed platinum nanoparticles although there are few agglomerates observed in Pt/EMWCNT. Platinum nanoparticles deposited on EMWCNT

and commercial CNT using isopropanol poses very poor loading and dispersion making isopropanol not a suitable solvent. Pt/C has a uniform particle size and spherical shaped arrangement of platinum nanoparticles on the carbon support. The Pt particles of Pt/C catalyst ranges between 2-4nm with an average diameter of 2.9nm. The general particle size of CNT supported Pt was found to be between 2-4.6 nm. The average particle size of Pt metals is given in Table 4.6 bellow

Table 4.6 Average particle size of Pt/MWCNT electrocatalysts

Pt/MWCNT	Mean Particle size by TEM (nm)	Mean Particle size by XRD (nm)
Pt/EMWCNT	2.8	2.5
Pt/LPGCNT	2.5	2.51
Pt/commercial CNT	2.75	2.5
Pt/EMWCNT in Isoprpanol	3.2	-
Pt/commercial CNT in Isoprpanol	2.9	-
Pt/C	2.7	2.3

The particle size calculated from the XRD data is small compared to that of TEM. This is due to the fact that, it is related to the area of coherent diffraction and in general can be smaller than actual crystallite size [160].

4.2.4 SURFACE AREA DATERNINATION OF SUPPORTED ELECTROCATALYSTS

The surface area of the Pt/MWCNT was measured using nitrogen physisorption by BET method. A summary of the results are tabulated in Table 4.7 below.

Table 4.7 BET surface area of MWCNT supported electrocatalysts

Pt/MWCNT	BET surface area (m^2/g)	Pore volume (cm^3/g)	BJH pore size (Å)
Pt/commercial CNT	251.62	1.16	208.98
Pt/LPGMWCNT	80.49	0.21	167.16
Pt/EMWCNT	56.80	0.14	119.300
Treated MWCNT			
LPGCNT	149.216	0.215975	1.9377
ECNT	170.564	0.140912	4.1551
Commercial CNT	191.706	0.674227	10.6227

The results in Table 4.7 show an increase in surface area of all the samples with the addition of platinum. Pt/commercial CNT has a high BET surface area. Pt/EMWCNT poses the smallest surface area, pore volume and pore size suggesting relatively dense particles with small porous structure. Increase of the total surface area of the MWCNT supports was observed upon addition of nanoparticles, this may be caused by the ultrasound procedure used during Pt deposition, breaking the CNT agglomerates and resulting in more separate CNTin the same mass and volume, thus more surface area. reduction of the external surface area as the Pt nanoparticles are being attached on the outer surface of the tube walls and could also be related to the formation of aggregates during sample preparation steps.

4.2.5 SUMMARY

The investigation of Pt nanoparticles supported on multi-walled carbon nanotube was initiated by elucidating the structure of the electrocatalysts. XRD results gave the particle size, lattice parameters, interplanar spacing and surface area. EDS and SEM were used for the composition and morphology of the electrocatalyst. SEM was limited to surface morphology due to its

inability for particle size measurements and TEM was used for particle size characterization. The particle size for Pt nanoparticles from XRD was close but smaller than the TEM results. It was believed that, this is due to the crystalline size relation to the area of coherent diffraction.TEM also proved high dispersion of Pt on the EMWCNT and LPGCNT. A trend of decreasing pore size of the catalysts as the surface area decreases was observed.

4.3 ELECTROCHEMICAL CHARACTERIZATION OF SUPPORTED ELECTROCATALYSTS

Electrocatalysts supported on multi-walled carbon nanotubes were investigated for their electrochemical characteristics such as activity, oxygen reduction reaction and tolerance towards methanol by Scanning Electrochemical microscopy and cyclic voltammetry. The electrochemical characteristics of the synthesized catalysts (Pt/MWCNT) were compared to those of commercial Pt/C catalyst. Only the electrocatalysts prepared by use of ethylene glycol as the solvent and reducing agent are tested for electrochemical activity because of the poor deposition and dispersion of Pt on the support during the deposition when isopropanol was used as confirmed by TEM.

4.3.1 TOPOGRAPHIC INFORMATION AND SURFACE ACTIVITY CHARACTERIZATION.

The analysis of the surface activity of electrocatalyst by SECM was conducted following the procedure given in chapter 3 section3.4.1. Activity of the Pt/MWCNT and Pt/C was also measured by mapping the surface of the electrocatalyst in SECM. Prior to mapping, Cyclic voltammetry was performed at an ultra-micro electrode. This was done in order to get the

potential to which the UME will be biased and the potential was found to be -0.73V vs Ag/AgCl. In order to investigate the topographical activity of the catalysts the distance between the UME and the substrate need to be known. Thus approach curves were conducted and all the catalysts posses the same response. A typical approach curve from one of the catalysts is shown in figure 4.8

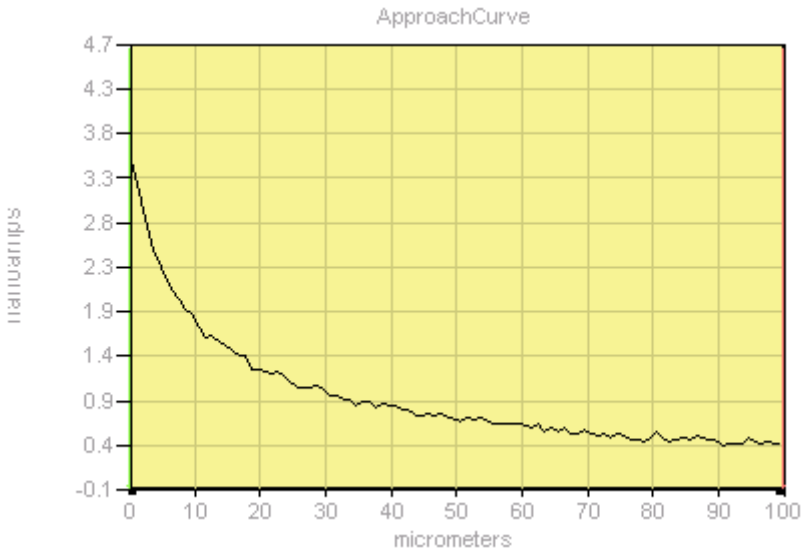

Figure 4.8 *Approach curve for Pt/ECNT (similar to other electrocatalysts including Pt/C)*

The shape of the approach curve above proved that the substrate is conductive. To get the suitable tip-substrate distance (d) where the UME tip will be probed for imaging, the ratio of d/a where a is the diameter of the UME must be close to unity (d/a =1) [161]. The tip-substrate distance for imaging was found to be 30µm. Images were then measured from Pt/MWCNT gas diffusion electrodes immersed in 0.5M sulfuric acid; the images are shown in figure 4.9 below.

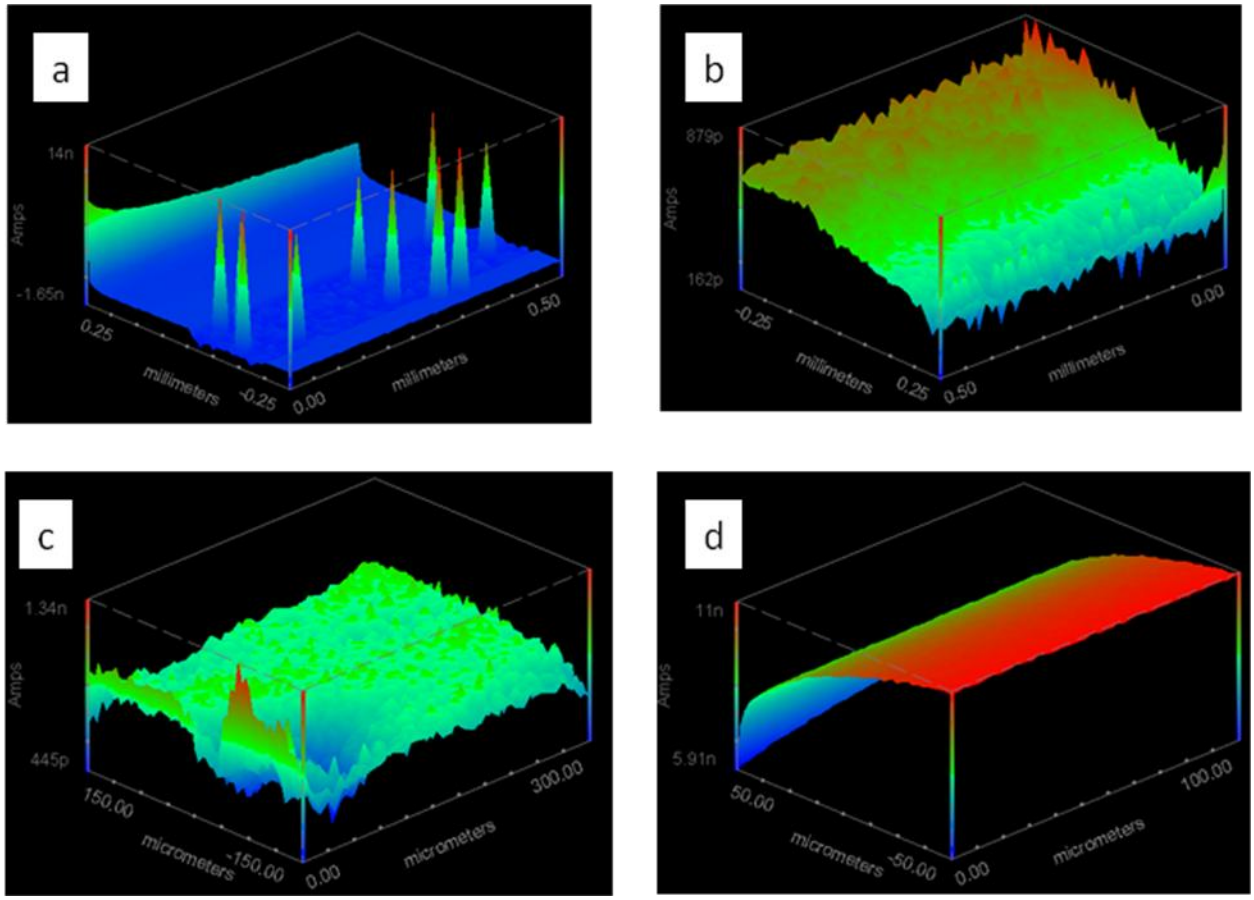

Figure 4.9 *SECM images of Pt/MWCNT (a) Pt/LPGMWCNT, (b) Pt/EMWCNT, (c) Pt/commercial CNT and (d) Pt/C*.

The SECM maps exhibit regions of varying positive feedback suggesting that some regions are more catalytic than others with high currents corresponding to Pt- rich areas. In all the Pt/MWCNT samples, the topography activity is not uniform proving the presence of Pt agglomerates in the samples. The activity, corresponding to the color, increased in the following order: red (high activity) > green (intermediate activity) > blue (low activity). Pt/LPGMWCNT shows the highest activity with current of 14nA and Pt/EMWCNT having the smallest current of

0.839 nA. Pt/C posses uniform dispersion of Pt with a current of up to 11nA. The point of contact during the positioning of the UME is observed as a disk like feature in Figure 4.9(c)

Topography and surface elemental distribution of the electrocatalysts were also investigated using PIXE. The images of elemental distribution mapping for Pt/MWCNT are presented in Figure 4.10

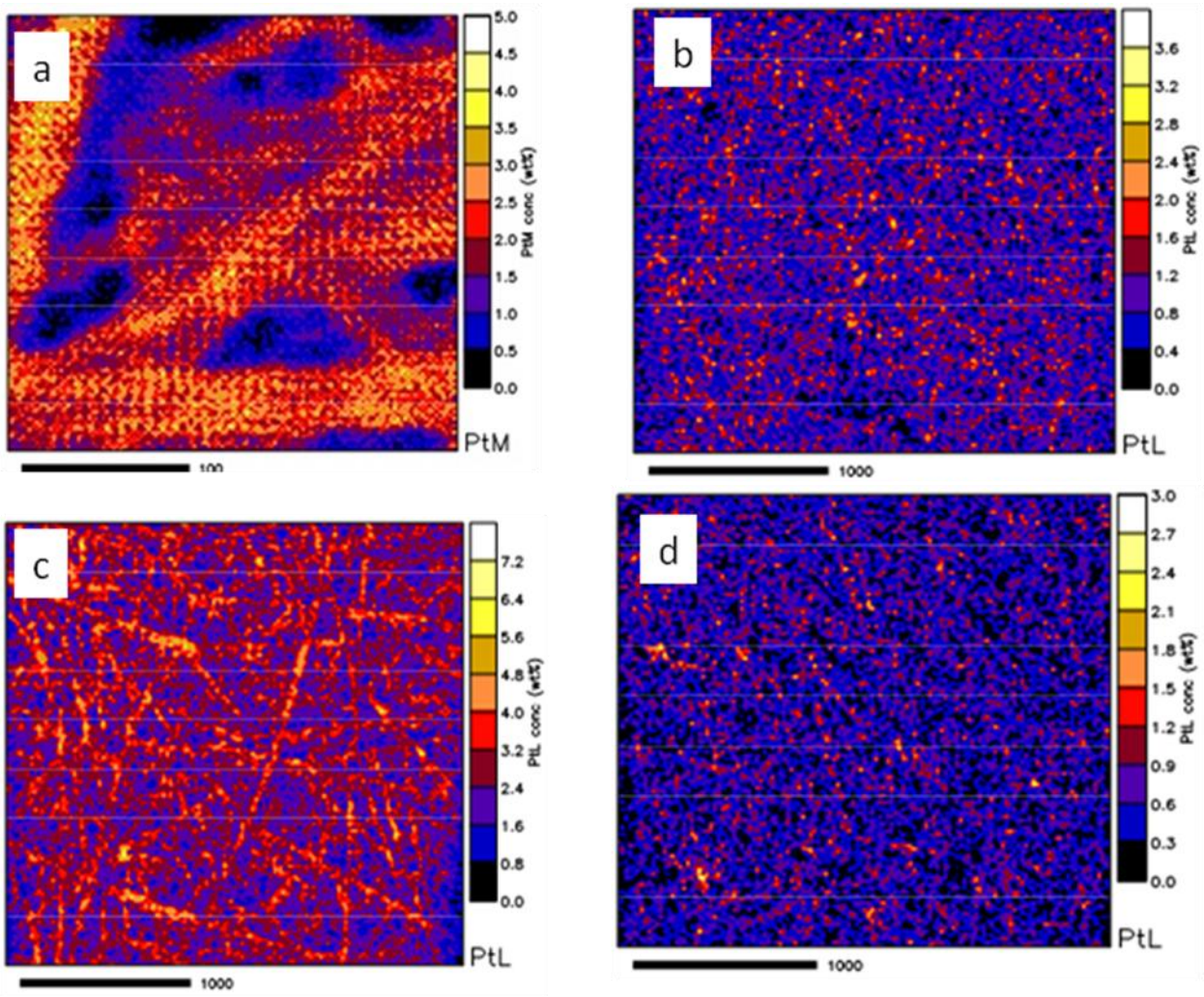

Figure 4.10 *PIXE maps of (a) Pt/commercial MWCNT, (b) Pt/EMWCNT, Pt/LPGCNT and (d) Pt/C.*

For PIXE analysis, the samples were sprayed on carbon paper. Figure 4.10 (a) shows non-homogenous distribution of Pt as it can be seen from the concentration bar that darker areas are of low or no Platinum regions. Sample (b) in the figure shows a very speckled appearance, of high Pt regions surrounded by very low Pt regions, which suggests that Pt is very agglomerated in the sample and a similar observation with sample (d). The dark areas are due to the structure of the substrate (carbon paper), because carbon paper is porous and made a network of carbon nanofibers that are not well oriented or aligned forming gaps in between the fibers. Thus the sample tends to only attach on the surface, making it difficult to achieve even distribution of the sample. Sample (c), PtLPGMWCNT shows a better distribution and concentration of Pt, but there is still a lot of high regions and low regions, so it is also very agglomerated.

4.3.2 ACTIVITY AND OXYGEN REDUCTION REACTION ON SUPORTED ELECTROCATALYSTS

The activity and oxygen reduction reaction of the catalysts was conducted using cyclic voltammetry. Methods used are detailed in section 3.4.2. Figure 4.11 shows cyclic voltammograms of electrocatalysts conducted in 0,5M H_2SO_4, scan rate of 50mVs^{-1} and in

potential range of -0.2V to 1V versus Ag/AgCl.

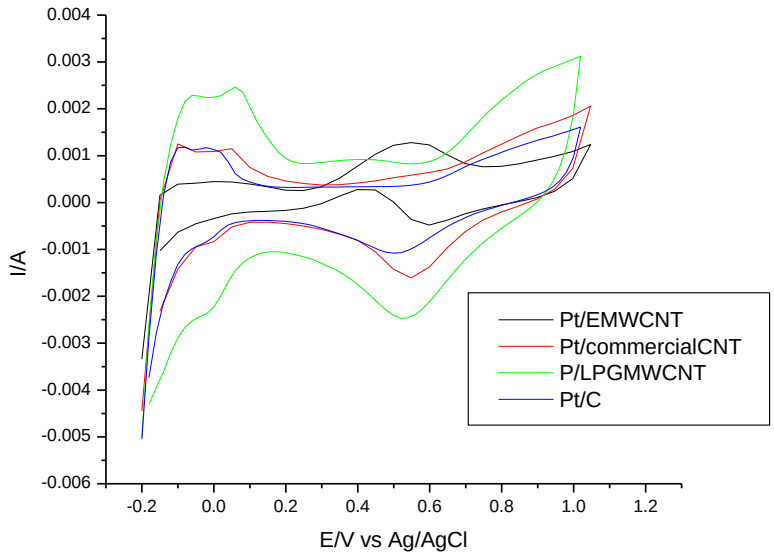

Figure 4.11 *Cyclic voltammogram of Pt/MWCNT catalysts 0.5 M H_2SO_4 solution de-aerated with N_2 for 30 minutes. Samples used were 0.25mg/cm^2 sprayed on carbon paper.*

The voltammograms in figure 4.11 above show well defined peaks of three distinct regions; hydrogen under-potential (Pt-H adsorption/desorption), electric al double layer and an oxide region consisting of the formation and reduction of Pt oxides except for Pt/EMWCNT. The Pt-Hydride adsorption peak potential appears from 0.200 to 0.0.09V for all catalysts, Pt-oxide reduction from 0.403 to 0.67V, Pt-oxide formation shows from 0.67 to 1V and the electric double layer from 0.09 to 0.403V. There is a slight shift of the reduction peak towards positive values observed in Pt/ECNT. Pt/LPGMWCNT has a significantly large activity compared to other electrocatalysts. The activity was in the order Pt/LPGMWCNT > Pt/commercial CNT > Pt/C > Pt/EMWCNT.

The active electrochemical surface area was calculated from the following equation [162, 163].

$$A_{EL} = Q_H / (0.21 \times 10^{-3} \times Lpt) \qquad \text{Equation: 4-1}$$

Where A = active surface area (m2/g), Q_H = hydrogen desorption peak, $0.21x10^{-3}$ = Charge required to oxidize a monolayer of H_2 on bright Pt (mC) and Lpt = Pt loading (mg/cm^2). The platinum loading was $0.25mg/cm^2$The active surface area is summarized in Table 4.3.2-1

Table 4.8 Active surface area of supported Electrocatalysts

Supported Catalyst	Q_H (mC)	ORR Activity (mA)	Active surface area, A_{EL} (m^2/g)	BET SA (m2/g)	TEM particle size (nm)	XRD particle size	SECM activity (nA)
Pt/LPGMWCNT	40.0	2.48	76.2	80.49	2.5	2.51	14
Pt/EMWCNT	9.3	0.005	17.1	56.80	2.8	2.5	0.839
Pt/commercialCNT	25.9	1.58	49.3	251.62	2.75	2.5	1.34
Pt/C	18.4	1.11	35.05	-	2.7	2.3	11

Pt/LPGMWCNT showed a higher electrochemical active area followed by Pt/commercial CNT. The high activity and active surface area of these catalysts may be attributed to the surface area of the support and to the platinum loading as proven by the EDS, Pt/LPGMWCNT had the loading of 19.8 and also on the particle size of Pt compared to Pt/commercialCNT. The ORR activity also increased with decreasing Particle size. This conclusion is confirmed by Myoung-ki, Parmigiani, Takasu and L. Geniès [164-165], who came to the same conclusion, that particle size does affect the ORR and that the potential of the ORR peak is decreased by decreasing particle

size. The results of E_{ORR} obtained from the CV study for the five catalysts correspond well with this conclusion.

4.3.3 OXYGEN REDUCTION AND METHANOL TOLARENCE INVERSTIGATION ON Pt/MWCNT

The behavior of the electrocatalyst towards oxygen reduction was investigated. During the experiment the electrolyte was saturated with pure oxygen and the experiment was cycled from 1 to -0.2V at 20mV/s in 0.5MH_2SO_4. The effect of methanol concentration was also monitored by cycling the electrodes in different concentrations of methanol containing H_2SO_4 solutions. Figure 4.12 shows a CV of the various Pt/MWCNT samples and Pt/C for comparison.

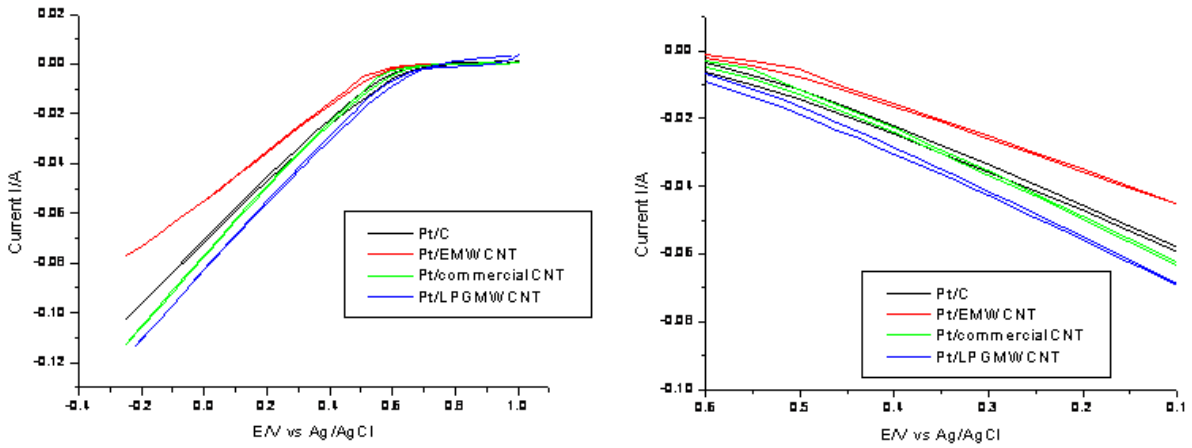

Figure 4.12 *Cyclic voltammograms of MWCNT supported Pt (a) oxygen reduction in O_2 saturated 0.5M H_2SO_4, (b) Plateau regions of (a).*

From figure 4.12 above, it is clearly observed that Pt/LPGMWCNT and Pt/commercial has the highest activity of 0.113 A towards ORR. Pt/EMWCNT has the lowest activity as observed in figure 4.11. The larger particle size contributes to the lower activity of Pt/EMWCNT.

4.3.4 EFFECT OF METHANOL CONCENTRATION ON MWCNT SUPPORTED PLATINUM ELECTROCATALYST

In direct methanol fuel cell, methanol diffuses through the membrane towards the cathode. In this section the effect of methanol is investigated. Different concentrations of methanol were added in the electrolyte to observe any changes in the ORR that may occur due to its presence in the cell. Figure 4.13 shows effect of methanol at different concentrations on Pt/MWCNT.

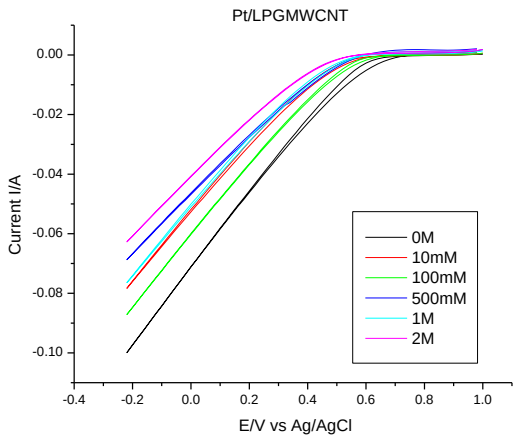

(a)

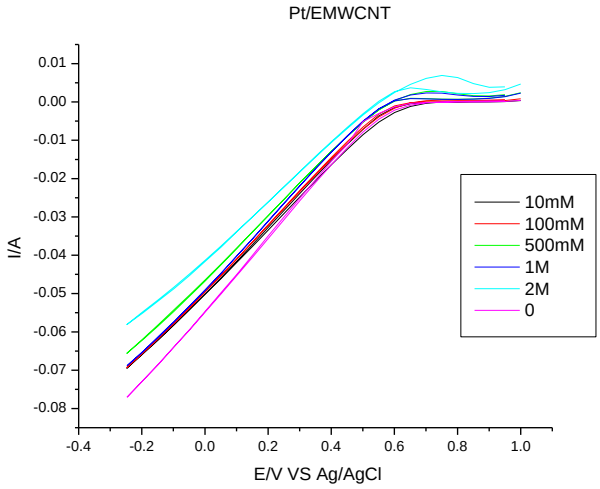

(b)

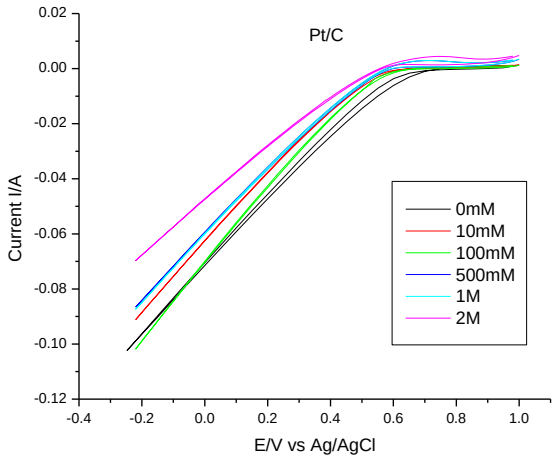

(c)

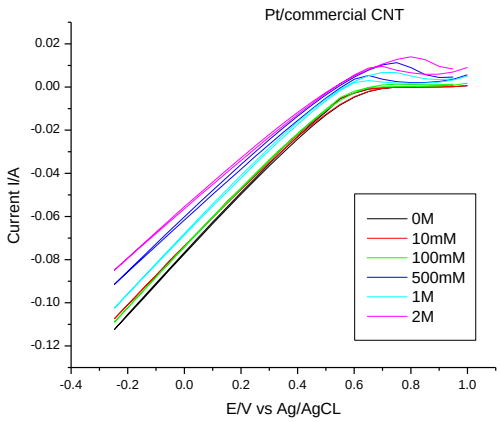

(d)

Figure 4.13 *Cyclic Voltammograms of oxygen reduction on (a) Pt/LPGMWCNT , (b) Pt/MWCNT, (c) Pt/C and (d) Pt/commercial CNT in 0.5M H_2SO_4 in different concentrations of methanol.*

A similar trend as in ORR is observed even in the presence of methanol as shown in figure 4.13 above. Pt/LPGMWCNT is the most active catalyst in the presence of methanol followed by Pt/commercial CNT. Pt/EMWCNT has the lowest activity towards methanol. The activity of the electrocatalysts decreases with an increase in methanol concentration. This is due to the competition of methanol oxidation and oxygen reduction reactions for the same platinum sites. The CV curves showed lower performance when methanol was added, the activity decreased from 10mM of methanol added indicating the influence of MOR on ORR. Methanol oxidation peak is observed in all the electrocatalysts when 500 mM methanol is added and increases with increasing concentration. Methanol oxidation peak potential is between 0.75 and 8.00V for all electrocatalyst and is at its maximum when 2M methanol is added. It can be seen that

Pt/EMWCNT has high methanol oxidation current compared to other catalysts, indicating high electrocatalytic activity towards methanol, hence making it a poor catalyst for ORR where the catalyst need to be methanol tolerant. Pt/LPGMWCNT and Pt/C are more tolerant towards methanol. The activity results of oxygen reduction are summarized in Table 4.9.

Table 4.9 Specific activity of MWCNT supported catalyst in different methanol concentrations.

Methanol concentration	Pt/LPGMWCNT (A/cm^2)	Pt/EMWCNT (A/cm^2)	Pt/commercial CNT (A/cm^2)	Pt/C (A/cm^2)
0M	0.09	0.068	0.090	0.088
0.01M	0.069	0.061	0.088	0.079
0.1M	0.078	0.061	0.088	0.088
0.5M	0.061	0.057	0.079	0.077
1M	0.68	0.060	0.080	0.077
2M	0.055	0.05	0.074	0.61

The activities in Table 4.9 above are normalized by the geometric area of the working electrode. The specific activity values clearly show that although Pt/MWCNT is tolerant towards methanol because of the low current for methanol oxidation peak, the activity significantly decreases with increasing concentration of methanol while activity of Pt/commercial CNT, with lager oxidation

peak current , is not greatly affected. Another observation is the low activity corresponding to the 500mM methanol solution compared to the higher concentration of 1M.

4.5 SUMMARY

Platinum catalysts supported on different carbon nanotubes have been evaluated for their electrocatalytic properties. It was found that the performance of the electrocatalysts depends largely on the structural properties of the catalyst metal, support material and the morphology of the electrocatalyst. Pt/MWCNT poses higher performances in most areas than Pt/C although Pt/C has the small particle size and high surface area confirmed using BET. This may be attributed to the MWCNT properties and the attachment of the Pt on the support material. Pt/LPGMWCNT proves to e the better catalyst for oxygen reduction.

5.1 CONCLUSION AND RECOMMENDATION

This research was based on finding a better catalyst that can improve oxygen reduction reaction (ORR) for the cathode electrode of the DMFC. It was confirmed from the Literature that supported electrocatalysts give better performance than unsupported, hence the choice of focusing on supported catalysts. The support material has to posses certain properties that will make it a suitable material to be used as support of the metal catalyst. Because of the properties needed for support material, multi-walled carbon nanotubes were used due to literature reports that have shown the superior performance of CNT, and exhibiting unique electronic, physical and mechanical properties. Platinum was used as it is the most active, well documented performance as electrocatalysts and national priorities in beneficiation of platinum resources. One challenge in using Platinum is the high cost of this catalyst which makes the DMFC expensive, hence the use of support material to reduce the amount of catalyst used and to minimize the adverse effects the presence of methanol on the cathode side of the cell caused by methanol crossover, which is another challenge faced by DMFC to which this study was focused on.

The experimental part of the research was initiated by the production of two sets of carbon nanotubes (CNT) by chemical vapor deposition method (CVD) using LPG and ethylene as carbon source. The CNT were named according to the carbon source used i.e. LPGMWCNT for MWCNT made using LPG, and EMWCNT for MWCNT made using ethylene gas. The CNT were characterized using a range of instruments; specifically SEM, TEM, XRD, AFM and EDS

for chemical composition. A purification and surface treatment procedure, based on methods in literature, was conducted using nitric acid and sulfuric acid mixture. A comparison was done with CNT before and after purification using and TEM and XRD analysis. The purity was confirmed, although small amounts of catalyst were observed by the EDS after acid treatments, and the type of CNT was confirmed to be multi-walled CNT. Both sets of MWCNT were observed to have hexagonal graphitic structure and outside diameter of 16-76 and 21-85 for LPGMWCNT and EMWCNT respectively, and 50nm diameter was observed with AFM which was within the range observed by TEM.

Platinum was deposited on the MWCNT by chemical deposition method (targeting 20wt% of Pt) using ethylene glycol (EG) as the solvent and reducingagent (polyol method) and for comparative purpose a formaldehyde reductant and isopropanol solvent were also used. It was observed from XRD and TEM that EG method showed small Pt particle size and better distribution/dispersion of various Pt on the MWCNT (LPGMWCNT, EMWCNT and commercial MWCNT). 20% Pt/C was characterized for comparison and wt% of 21.8, 19.10 and 16.74 for Pt/ECNT, Pt/LPGCNT and Pt/commercial CNT respectively was achieved. Small particle sizes in low nanometer range were observed from TEM and XRD data.

For electrochemical characterization of the nanoparticle electrocatalysts, SECM and CV were used. The results from SECM maps show Pt agglomerates for all electrocatalysts except Pt/C. SECM did not give satisfactory results due to its low resolution and was seen to be a technique that gave limited information for this study. PIXE was also conducted for discrimination of elemental composition of the electrocatalysts. Images from PIXE were seen to be in agreement with the TEM micrographs on the dispersion of Pt metal.

The activity of the electrocatalysts was measured by CV. In a nitrogen purged sulfuric acid electrolyte, Pt/LPGMWCNT showed a large hydrogen adsorption-desorption and oxygen reduction currents. The order of ORR was Pt/LPGMWCNT > Pt/Commercial CNT > Pt/C > Pt/EMWCNT. This can be attributed to the Pt wt% in the case of Pt/LPGMWCNT and the surface area in Pt/commercial CNT and also the treatment of the MWCNT play a significant role on anchoring the Pt metal onto the MWCNT surface. Pt/C activity was lower although the surface area was high, this is due to micro-pores of Pt/C which are not easily accessible for the electrochemical processes. Pt/EMWCNT had high platinum loading but very small surface area of the support and poor distribution thus is the least active.

The Pt/MWCNT electrocatalysts were tested for their tolerance towards methanol which negatively affects the performance of the cathode electrode in DMFC. It was observed that the activity of the electrocatalysts decreases with an increase in methanol concentration. Methanol oxidation peak was observed when 500mM of methanol was added to the electrolyte and high methanol oxidation peak currents were more significant on Pt/EMWCNT and Pt/commercial CNT making them very sensitive towards methanol. The activity of the Pt/commercial is not greatly affected by the presence of methanol though high methanol oxidation peak currents were observed. In this study Pt/LPGMWCNT was the best catalyst for ORR compared to other electrocatalysts followed by Pt/commercial CNT. It is concluded that carbon nanotubes are good support material for Pt electrocatalysts for DMFC cathode electrode. The surface area of the catalyst for preparation of carbon nanotubes must be evaluated as the size of their diameter depends on it. There needs to be an understanding on the behavior of Pt/commercial CNT

towards methanol tolerance. Testing the performance of the LPG/MWCNT on the direct methanol fuel cell is recommended.

REFERENCES

[1] Beder S. The hole story: Ozone depletion research in the areas of medical, biological and veterinary science, physics pharmacy and physiology. http://www.herinst.org/sbeder/HoleStory/hole.html

[2] Chlorofluorocarbons: *Chemical activity of CFCs* http://science.jrank.org/pages/1442/Chlorofluorocarbons-CFCs-Chemical-activity-CFCs.html

[3] The hidden cost of fossil fuels: *Union of Concerned Scientists*. http://www.ucsusa.org/clean_energy/technology_and_impacts/impacts/the-hidden-cost-of-fossil.html

[4] Electrochemical energy and conversion: *Electrochemistry* http://www.chem1.com/acad/webtext/elchem/ec6.html.

[5] Bockris J. O'M, Amulya K.N. Reddy. Modern electrochemistry: *Electrodics in chemistry, engineering, biology, and environmental science.*

[6] Energy, Heat, and Temperature: *An introduction for beginning chemistry.* *http://www.chem1.com/acad/webtext/pre/enheat.html*

[7] Energy Efficiency and Renewable Energy: *Fuel Cell Technologies Program.* http://www1.eere.energy.gov/hydrogenandfuelcells/

[8] Peter Rode: investigation of proton conducting polymers and gas diffusion electrodes in the polymer electrolyte fuel cells. Doctorial Thesis: Department of Chemical Engineering and Technology (2004)14.

[9] Rhalph and Hogarth. *Platinum Metals Revolution* 4 (2002)146-164

[10] Fuel Cells 200: The Online Fuel Cell Information Resource http://www.fuelcells.org/basics/types.html

[11] Larminie J. and Dicks A. *Fuel cell systems Explained*, 2nd Edition (2003), John Wiley and Sons Ltd.

[12] Holland B. Zhu JG. Jamet L. *Fuel Cell Technology and Application* (2007)

[13] Allan J. Jacobson. *Chemistry of Materials* 3, 22 (2010) 660–674

[14] Fuel cells: Collecting history of Solid Oxide Fuel Cells. http://americanhistory.si.edu/fuelcells/so/sofcmain.htm

[15] Stambouli A.B, Traversa E. *Renewable and Sustainable Energy Reviews* 6 (2002) 433–455

[16] Eileen J. De Guire. Review article Solid Oxide Fuel Cells http://www.csa.com/discoveryguides/fuecel/overview.php

[17] Bohmed O, Leidich F. U, SalgeH. J. and Wendt H. *International Journal of hydrogen Energy* 19 (1 994) 4, 349- 355.

[18] Bove R. Mereno A. McPhail S. *JRC Scientific and Technical Reports* (2008) 6-42

[19] Crawley G. Molten Carbonate Fuel Cells (MCFC). *Fuel Cell Today* (2007).

[20] Renewable Energy Technologies, Molten carbonate fuel cells.

http//www.MoltenCarbonate FuelCells.com

[21] Walsh B and Wichet R. *National Institute of Building Sciences* (2010)

[22] Methew M. *Mench Fuell cell engines*, John Wiley and Sons, 2008 - Technology & Engineering - 515.

[23] Nigel Sammes, Roberto Bove, Knut Stahl. *Current Opinion in Solid State and Materials Science* 8 (2004) 372–378.

[24] Crawley G. Alkaline Fuel Cells, *Fuel Cell Today* (2006).

[25] Verma A, Basu S. *Journal of Power Sources* 174 (2007) 180–185.

[26] Kordesch K. Hacker V. Gsellmann J. Cifrain M. Faleschini G. Enzinger P. Fankhauser R. Ortner M. l Muhr M. Robert R. Aronson. *Journal of Power Sources* 86 (2000)162–165.

[27] Ramani V. H. Russell K. and James M. Fenton. *The Polymer Electrolyte Fuel Cell*.

[28] Crawley G. Proton Exchange Membrane (PEM) Fuel Cells, *Fuel Cell Today* (2006)

[29] Fuel cells. http://www.energysolutionscenter.org

[30] Park G. Yang, Yoon, Lee and Kim. *International Journal of Hydrogen Energy* 28 (2003) 645-650

[31] Cruickshank J. Scott K. *Journal of Power Sources* 70 (1998) 40-47

[32] Salgado J. R. C. Antolini E. Gonzalez E. R. *Journal of Applied Catalysis B*: Environmental 57 (2005) 283-290.

[33] Chu D. Jiang R. *Electrochimica Acta* 51 (2006) 5829–5835

[34] Energy Efficiency & Renewable Energy, fuel cell technologies program http://www1.eere.energy.gov/hydrogenandfuelcells/fuelcells/fc_parts.html

[35] Ren X. Zelenay P. Thomas S. John Davey, Gottesfeld S. *Journal of Power Sources* 86 (2000) 111–116

[36] Shyu R. F. Yang H. Lee J. *Microsystem Technology* 15 (2009)1265–1271.

[37] Yang H, Zhao T.S. *Electrochimica Acta* 50 (2005) 3243–3252

[38] Manthiram A. Materials and manufacturing challenges of direct methanol fuel cell. The WSTIAC Quarterly 9, 1 69-74. http://ammtiac.alionscience.com/quarterly

[39] Shukla A.K. and Raman R.K. *Annu. Rev. Mater. Res*. 33 (2003) 155–68

[40] ElectroPhen™ conductive composites for bipolar plates. http://www.fuelcellmarkets.com/bac2 conductive composites/1,1,12899.html.

[41] Middelman E. Kout W. Vogelaar B. Lenssen J. de Waal E. *Journal of Power Sources* 118 (2003) 44–46

[42] Anghel V. Stefanescu I. Varlam M. Culcer M. *Nationa Hydrogen and Fuel Cell Center* (2010)

[43] Chepuri R. K. Rao. Trivedi D. C. *Coordination Chemistry Reviews* 249 (2005) 613-631.

[44] Thomas C. Ren X. Gottesfeld S. Zelenay P. *Electrochimica Acta Journal* 47 (2002) 3741-3748

[45] Philip H. Rieger. *Electrochemistry* (1987) 58

[46] Yaun W. Scott k. Cheng H. *Journal of Power sources* 163 (2006) 323-329

[47] Hacquard A. Improving and Understanding Direct Methanol Fuel Cell (DMFC) Performance. A Thesis submitted to the faculty of *Worcester Polytechnic Institute* In partial fulfillment of the requirement for the Degree of Master of Science In Chemical Engineering 2005

[48] Sandhu S.S. Crowther R.O. Krishnan S.C. Fellner J.P. *Electrochimica Acta* 48 (2003) 2295-2303.

[49] Hollingera A.S, Maloney R.J, Jayashree R.S, Natarajanc D, Markoskic L.J, Kenisa P.J.A. *Journal of Power Sources* 195 (2010) 3523–3528.

[50] Valdez T. I. and Narayanan S.R. *Jet Propulsion Laboratory, California Institute of Technology,* 4800 Oak Grove Drive, Pasadena.

[51] Munichandraiah N, McGrath K. G.K, Prakash S, Aniszfeld R, George A. Olah. *Journal of Power Sources* 117 (2003) 98–101

[52] Ramya K. Dhathathreyan K S. *Journal of Electroanalytical Chemistry* 542 (2003) 109-115

[53] Surampudi, S.R. Narayanan, E. Vamos, H. Frank, G. Halpert, A. Laconti, J. Kosek, G.K. Prakash S. and Olah G.A. *journal of Power Sources* 47 (1994) 377.

[54] Jung H D. Lee C H. Kim C S. Shin R D. *Journal of Power Sources* 71 (1998) 169-173

[55] Heinzel A, Barrag´an V.M. *Journal of Power Sources* 84 (1999) 70–74.

[56] Qi Z. and Kaufman A. *Journal of Power Sources* 110 (2002) 177-185

[57] Antonino S. A. Baglio V. and Antonucci V. *Electrocatalysis of Direct Methanol Fuel Cells*. Edited by Hansan Liu and Jiujun Zhang: Copyright (2009) 7 WILEY-VCH Verlag GmbH & Co. KGaA, Weinheim.

[58] Fernandas J.B. *Electrocatalysis*, Department of Chemistry,University of Goa, Goa.

[59] Young-ping G. Hui H. Wen-kui Z. *Transactions of Nonferrous Metals Society of China* 17 (2007)214-219

[60] Hoogers G. *Handbook of Fuel Cell Technology* (2003) by CRC press

[61] Metikos-Hukovic M. Babic R. Piljac Y. J*ournal of New Materials for Electrochemical Systems* 7 (2004) 179-190

[62] Kauranen P.S, Skou E. *Journal of Electroanalytical Chemistry* 408 (1996) 189-198

[63] Chitturi venkateswara rao,on the search for efficient cataltyst for oxygen reduction reaction a thesis by the department of chemistry,Indian institute of technology (2008) 11

[64] Tseung, P k D. and Hobbs B. S. High Activity Fuel Cell Electrodes, THE INFLUENCE OF ELECTROCATALYST SUPPORTS By A. C. C., Chemistry Department, The City University, London).

[65] Shukla A. K, Neerget M, Parthasarathi B, Jayaram V, and Hedge M.S. *Journal of Electro-analytical Chemistry* 504 (2001) 111

[66] Fuel Cell Hand book, Fourth edition, EG & G. Services Parsons, Inc. 2000

[67] Gattrel M. MacDougall B. Reaction Mechanisms of Oxygen Reduction, Handbook of Fuel Cells: Fundamentals, Technology and Application. John Willey and Sons 2,453

[68] Muller L. and Nekrasov L.N. *Electrochimica Acta* 9 (1964) 1015.

[69] Damjanovic A, Genshaw M.A. and Bockris J.O.'M. *Journal of Chemical. Physics* 45 (1966) 4057.

[70] Wroblowa H.S, Pan Y.C. and Razumney G. *Journal of Electroanalytical Chemistry* 69 (1976) 195.

[71] Appleby A.J and Savy M. *Journal of Electroanalytical* Chemistry 92 (1978) 15.

[72] Zurilla R.W, Sen R.K and Yeager E. *Journal of Electrochemical Society* 125 (1978) 1123.

[73] Geisteiger HN. Markovic N. Ros PN. Cain EJ. *Journal of Physical Chemistry* 97 (1993) 12020

[74] Kirschenmann M. Wohrle D. Vielstich W. Bunsengers Ber. *Journal of Physical Chemistry* 92 (1988) 1403.

[75] Yeager E. *Electrochimica Acta* 29 (1984)1527

[76] Wang J. T, Sun G. Q and Savinell R. F. *Journal of Applied Electrochemistry* 28 (1998) 1087-1093

[77] Maillard F. Martin M. Gloaguen F. Leger J. M. *Electrochimica Acta* 47 (2002) 3431

[78] Shukla A. k. Raman R. K. Choundhuri N. A. Priolkar K. R. Serode P. R. Emura S. Kumashiro R. *Journal of Electroanalytical chemistry* 563 (2004) 181

[79] Zhang J. PEM Fuel Cell Electrocatalyst and Catalyst layers 611

[80] Tsivadze A, Tarasevich M. R, Bogdanovskaya V. A, Kuznetsova L. N, kapustina N. A, Modestov A. D. *Doklady Chemistry* 1. 410 (2006) 154-157

[81] Tarasevich M. R, Bogdanovskaya V. A, Kuznetsova L. N, Modestov A. D, Efremov B. N, Chalykh A. E, Chirkov Yu. G, Kapustina N. A, Ehrenburg M. R. *Journal Applied Electrochemistry* 37 (2007) 1503–1513

[82] Baglio V, Stassi A, Blasi A, D'Urso C, Antonucci V, Arico A. S. *Electromicha Acta* 53 (2007)1360-1364

[83] Xiong L, Kannan A. M, Manthiram M. *Journal of Electrochemical Communications* 4 (2002) 898

[84] Drillet H. E. A, Friedemann J, Kotz R, Schnyder B, Schmidt V. M. *Electrochimica Acta* 47 (2002) 1983

[85] Yang H. Alonso-Vante N. Leger JM. Lamy C. *Journal of Physical Chemistry B* 108 (2004) 1938

[86] Glass J. T, Cahen G. L, Stoner G. E, Taylor E. J. *Journal of Electrochemical Society* 134 (1987) 58

[87] Neto AO. Perez J. Gonzalez ER. Ticianelli EA. *Journal of New Materials for Electrochemical Systems* 2 (1999) 189

[88] Paffett M. T, Berry G. S, Gottesfeld S. *Journal of Electrochemical Society* 135 (1998) 1431

[89] Toda T, Gorashi H, Uchida H, Watanabe M. *Journal of electrochemical Society* 146 (1999) 3750

[90] Beard B C. Ross P N. *Journal of Electrochemical Society* 137 (1990) 336

[91] Bregoli L. J. *Electrochimica Acta* 23 (1978) 489

[92] Hwang J. T, Chung J .S. *Electrochimica Acta* 38 (1993) 2715

[93] Bett J, Lundquise J, Washington E, Stoneheart P. *Electrochimica Acta* 18 (1973) 343

[94] Min M, Cho J,Cho K, Kim H. *Electochimica Acta* 45 (2000) 4211-4212

[95] Kinoshita K. electrochemical Oxygen Technology, *Electrochemical Society* (1992) 113 online book

[96] Antolini E. *Applied Catalysis B*: Environmental 88 (2009) 1–24

[97] Antolini E and Gonzalez E. R. *Solid State Ionics* 180 (2009) 745-769

[98] Wohler O, von Sturm F, Wege E, von Kienle H, Voll M, Kleinschmit P, in: W. Gerhartz (Ed.), Ullmann's Encyclopaedia of Industrial Chemistry, vol. A5, VCH, Weinheim, (1986) 95.

[99] Paul V. Shanahana, Lianbin Xua, Chengdu Liang, Mahesh Waje , Sheng Daic,, Yan Y.S, *Journal of Power Sources* 185 (2008) 423–427

[100] Johnson Matthey^{TM} Catalyst Datasheet HiSPEC online

[101] Ray H. Baughman, Anvar A. Zakhidov, Walt A.de Heer. Carbon Nanotubes-the route towards Applications. *Science compass review.*

[102] Teri Odom, Jin-Lin Huang, Philip Kim and Charles M. Lieber. *Journal of Physical Chemistry B* 104 (2000) 2794-2809

[103] Honjie D. *Surface Science* 500 (2002)218-241.

[104] Erik T. Thostensona, Zhifeng Renb, Tsu-Wei Choua, *Composites Science and Technology* 61 (2001) 1899–1912)

[105] Foley M. Carbon nanotubes 101. A practical guide to understanding their properties, Application, Production Methods, Markets and Utilities (2006) Cheap Tubes Inc.

[106] P. M. Ajayan *Chem. Rev*. *99 (*1999) 1787-1799

[107] Lijima S. *Nature* 354 (1991) 56-58

[108] Wenzhen L. Changhai L. Zhou W. Qiu J. Zhenhua Z. Sun G. and Xin Q. *Journal of Physical Chemistry B* 107 (2003) 6292-6299

[109] Reyhania A, Mortazavi S. Z, Nozad Golikand A, Moshfegha A. Z, Mirershadi S. *Journal of Power Sources* 183 (2008) 539–543

[110] Ebbesen TW. Lezec HJ. Hiura H. Bennett JW. Ghaemi HF.Thio T. *Nature* 382 (1996) 54

[111] Lee K. M, Li L. C, Dai L. M. *Journal of American Chemical Society* 127 (2005) 142

[112] Kouravelou K.B. and Sotircho S.V. *Review in Advanced Materials Sciences* 10 (2005) 243-248

[113] Tsai Y. Hong Y. *Journal of Solid State Electrochemistry* 12 (2008) 1293-1299

[114] Girishkumar G. Hall T. D. Vinodgopal K. Kamat P. V. *Journal of Physical Chemistry B* 110 (2006) 107–114.

[115] Shimizu K. Wang J. S. and Chien M. Wai. *Journal of Physical Chemistry A* 114 (2010) 3956–3961.

[116] Park J. Kim M. J. Huh Y. Lee J.Y. No S.K. *Chemical Physics Letters* 327 (200) 277-273

[117] Antisari M. V. Marazzi R. and Krsmanovic R. *Carbon* 12,41 (2003)2393-2401

[118] Qiu H. Shi Z., Guan L. You L. Gao M. Zhang S. Qiu J. Gu Z. *Carbon* 44 (2006) 516-521

[119] Gilbert D. Nessim. *Nanoscale* 2 (2010) 1306-1323

[120] Lee C. J. Park J. H. Park J. *Chemical Physics Letters* 323 (2000) 560–565

[121] Jining X. Mukhopadyay K. Yadev J and Varadan V. K. *Smart Material Structure* 12 (2003) 744–748

[122] Chen C. Dai Y. Huang J. G. Jehng J. *Carbon* 44 (2006) 1808–1820

[123] Christian P. Deck, Gregg S.B. Mckee, and Kenneth S. Veccohio. *Journal of Electronic Materials* 2, 35 (2006).

[124] Bom D. Andrews R. Jacques D. Anthony J. Chen B. Meier M. S. and Selegue J. P. *Nano Letters* 6, 2 (2002) 615-619

[125] Beard B C. Ross P N. *Journal of Electrochemical Society* 137 (1990) 336

[126] Ndungu P, Nechaev A, Khotseng L, Onyegebule N, Davids W, Mohammed R, Vaivars G, Bladegroen B, Linkov V. *International Journal of Hydrogen Energy* 33 (2008) 3102 – 3106

[127] Yangchuan Xing. *Jornal of Physical. Chemistry B* 108 (2004), , 19255-19259

[128] Dr. William H. Heidcamp. The Microscope - Introduction, (available on line) http//homepages.gac.edu/cellab/chpts/chpt1/intro/htm

[129] Dougal G. McCulloch. Electron Microscopy – Introduction. (Available on line) http://encyclopedia.jrank.org/articles/pages/1129/Electron-Microscopy.html

[13o] Susan Swapp. Geometrical instrumentation and analysis. (Available on line) http://serc.carleton.edu/research_education/geochemsheets/techniques/SEM.html

[131] Prabhuram. J, Zhao. T.S, Wong. C.W, Guo. J.W. *Journal of Power Sources*, 134, 1 (2004) 1-6.

[132] Barbara L Dutrow, Louisiana State University ,Christine M. Clark, Eastern Michigan University. X-ray Powder D iffraction (XRD) Geochemical Instrumentation and Analysis.

[133] Terence A. *Particle size measurement*. Second Edition 100 (1997) 191

[134] Fagerlund G. *Matieriauxet Constructions*. 6 , 33 (1973) 239-245

[135] Surface Science Techniques. UK surface analysis forum (available on Line) http://www.uksaf.org/tech/afm.html

[136] Robert A. Wilson and Heather A Bullen. Introduction to Scanning Probe Microscopy: *Basic Theory Atomic Force Microscopy* (2006) 2-6

[137] Govil I. M. *Current Science* 80, 12 (2001) 1542-1549

[138] Rueter W, Lurio A, Cardone E. and Ziegler J. F. *Journal of Applied Physics* 46 (1975) 3194

[139] Luis Diaz –Baliote, Mario Alpuche-Aviles and David O-Wipf. *Journal of Electroanalytical Chemistry*. 604 (2007) 17-25

[140] Cynthia G. Zoski, Nafeesa Simjee. *Journal of Analytical Chemistry* 76 (2004) 62-72

[141] Laforge F. Electrochemistry Encyclopedia: Scanning Electrochemical Microscopy. (available on line) http://electrochem.cwru.edu/encycl/art-m04-microscopy.htm

[142] Fu-Ren F. Fan, Jose Fernandez, Biao Liu, Janine Mauzeroh. Scanning Elechtrochemical Microscopy, *Handbook of electrochemistry* (2007)471

[143] Anna L. Baker, Julie V. Macpherson, Cristopher J. Selvine and Patrick R. Unwin. *Journal of Physical Chemistry B* 102 (1998) 1586-1598

[144] Bard A. J, Faulkner L. R. Electrochemical Methods, Fundamentals and Applications, John Wiley and Sons, New York, 1980

[145] Wang Y. Wu J. Wei F. *Carbon* 41 (2003) 2939–2948

[146] Wei F. Zhang Q. Qian Wei-Zhong, Yu H. Wang Y. Guo-Hua Luo, Xu G. Wang D. Selected papers from the UK-China Particle Technology Forum; Leeds UK 1, 183 (2008) 10-20.

[147] Danafar F. Fakhru'l-Razi A. Mohd Amran Mohd Salleh, Dayang Radiah Awang Biak, A review, *Chemical Engineering Journal* 1-2, 155, (2009) 37-48.

[148] Rosca I. D. Watari F. Uo M. Akasaka T. *Carbon* 43 (2005) 3124–3131

[149] Xu H.F. Lin Y.Z. Qiu.Y. L. Tang Q. *Chinese Journal of Catalysis* 2, 24 (2003) 143-148.

[150] Chia-Ming Chen, Yong-Ming Dai, Jenn Gwo Huang, Jih-Mirn Jehng *Carbon* 44 (2006) 1808–1820.

[151] Niu J. J. Wang J. N. Solid State Sciences 10 (2008) 1189 -1193

[152] Kai Yanga, Haibo Hanb, Xifeng Pana, Na Chena, Mingyuan Gua. *Journal of Physics and Chemistry of Solids* 69 (2008) 222–229,

[153] Lau C. H. Cervini R. Clarke S. R., Markovic M.G. Matisons J. G. Hawkins S. C. Huynh C. P. Simon G. P. *J Nanopart Res* 10 (2008) 77–88

[154] Vielstich W, Lamm A, Gasteiger H, "Handbook of Fuel Cells, Fundamentals Technology and Applications", volume 2 (2005) 508, Printed and bound in Great Britain by Antony Rowe, Chippenham, Wiltshire.

[155] Saito T. Matsushige K. Tanaka K. *Physica* B 323 (2002) 280–283

[156] Prabhuram J, Zhao T. S, Tang Z. K, Chen R. and Liang Z. X. *Journal of Physical Chemistry. B* 110 (2006) 5245-5252.

[157] Kim Y.I. Soundararajan D., Park C.W. Kim S.H. Park J.H. Ko J.M. *International Journal of Electrochemical Science.* 4 (2009) 1548 – 1559.

[158] Oishi K. and Savadogo O. *Journal of New Materials for Electrochemical Systems* 11 (2008)221-227.

[159] Pozio A. De Francesco M. Cemmi A. Cardellini F. Giorgi L. *Journal of Power Sources* 105 (2002) 13–19.

[160] Nicholson P.G. Hou S. Z. Hinds G. Wain A.J.Turnbull A. *Electrochimica Acta* 54 (2009) 4525–4533.

[161] Zhaolin L. Lee J. Y. Chen W. Han M. and Gan L. M. *Langmuir* 20 (2004) 181-187

[162] Prabhuram J. Zhao T. S. Tang Z. K. Chen R., and Liang Z. X. *Journal of Physical Chemistry B* 110 (2006) 5245-5252

[163] F. Parmigiani, E. Kay, P.S. Bagus, J. *Electron Spectrose. Relat. Phenom*, 39 (1990) 50

[164] Frelink, W. Visscher, J.A.R. Van Veen, Journal Electroanalytic Chemistry. 65 (1995) 385

[165] Min M.K. Cho J. Cho K. Kim H. *Journal of Electrochimica Acta*. 45 (2000) 4211-4217,

[166] Geniès L. Faure R. Durand R. *Journal of Electrochemica Acta*. 44 (1998)1371-1327

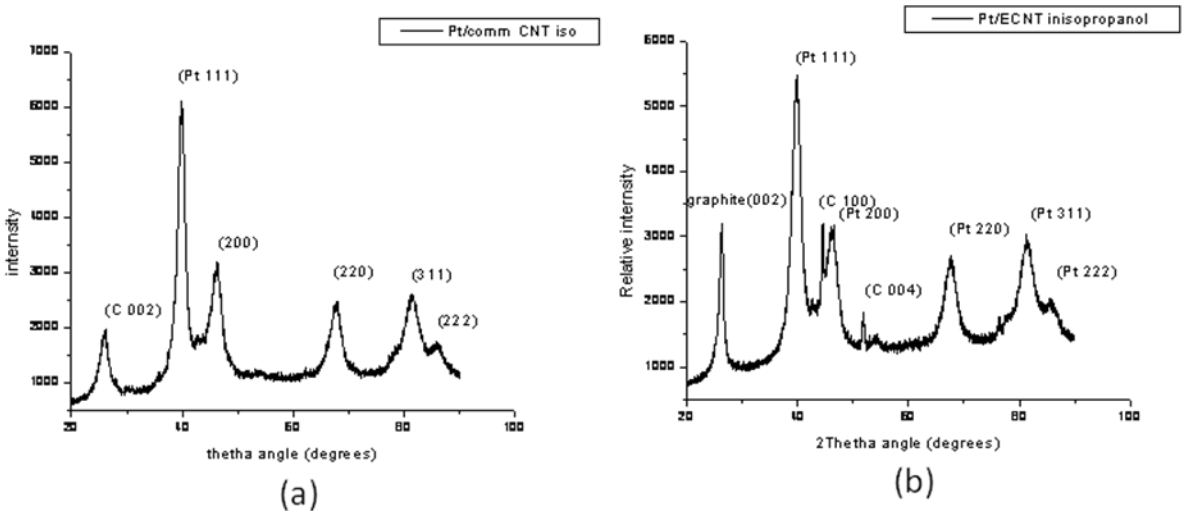

APPENDIX A. XRDmicrographs of (a) Pt/commercial CNT and (b) Pt/ECNT synthesized in isopropanol

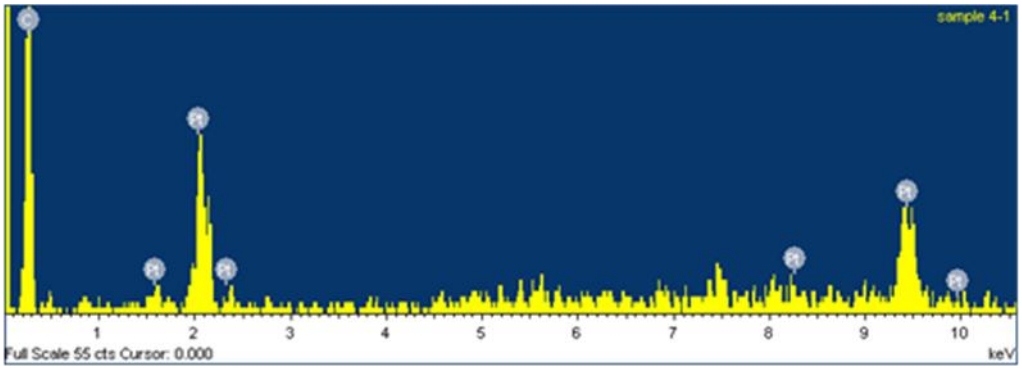

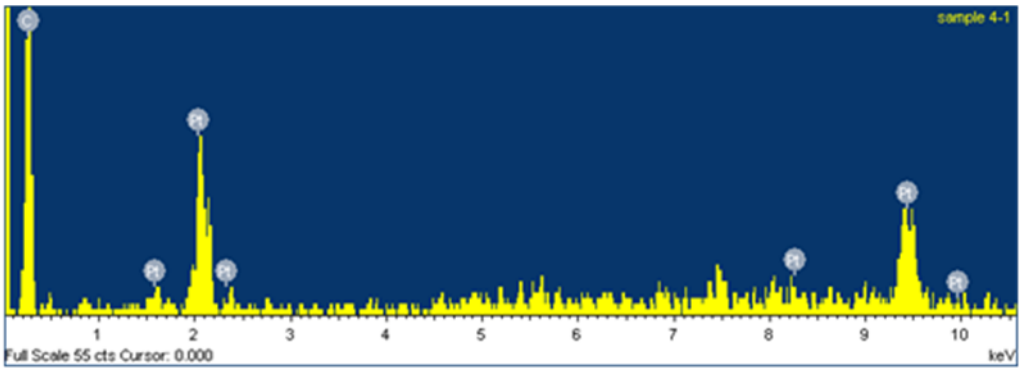

(b)

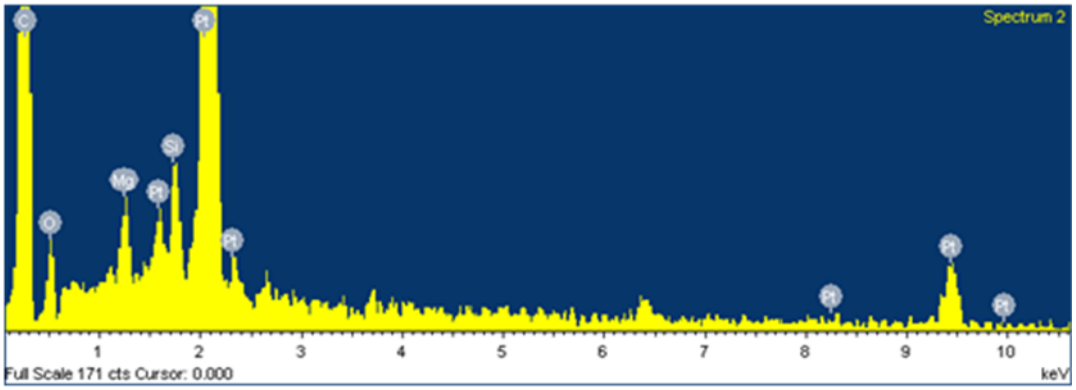

(c)

APPENDIX B EDS elemental analysis of (a) Pt/LPG MWCNT, (b) Pt/EMWCNT and (c) Pt/commercial CNT.